On Numerical Models of Calcium-Induced Calcium Release

by

Andrew T. L. Nixon

B.S. Mathematics, Rensselaer Polytechnic Institute; Troy, NY, 2008

B.S. Physics, Rensselaer Polytechnic Institute; Troy, NY, 2008

M.S. Applied Mathematics, Rensselaer Polytechnic Institute; Troy, NY, 2008

A dissertation submitted in partial fulfillment of the

requirements for the degree of Doctor of Philosophy

in The Division of Applied Mathematics at Brown University

PROVIDENCE, RHODE ISLAND

May 2015

This dissertation by Andrew T. L. Nixon is accepted in its present form by The Division of Applied Mathematics as satisfying the dissertation requirement for the degree of Doctor of Philosophy.

Date_____ _____

Björn Sandstede, Ph.D., Advisor

Recommended to the Graduate Council

Date_____ _____

Anastasios Matzavinos, Ph.D., Reader

Date_____ _____

Martin Maxey, Ph.D., Reader

Approved by the Graduate Council

Date_____ _____

Peter M. Weber, Dean of the Graduate School

Vitae

Professional Preparation

Rensselaer Polytechnic Institute	Mathematics	B.S., *summa cum laude*, 2008
Rensselaer Polytechnic Institute	Physics	B.S., *summa cum laude*, 2008
Rensselaer Polytechnic Institute	Applied Mathematics	M.S., 2008
Brown University	Applied Mathematics	Ph.D., expected 2015

Appointments

Teaching Assistant, Rensselaer Polytechnic Institute	Fall 2007 - Spring 2008
Research Assistant, Brown University	Fall 2010 - present
Teaching Assistant, Brown University	Fall 2011 - Spring 2012,
	Fall 2013 - present

Publications

M. Crosskey, A. Nixon, L. Schick, G. Kovačič. *Invisibility cloaking via non-smooth transformation optics and ray tracing.* Physics Letters A, **375**, 1903-1911 (2011).

Presentations

Invisibility cloaks for asymmetric objects. SIAM Annual Meeting, Denver, 2009.

Teaching Experience and Training

MATH 1010-1020: Calculus I + II, Teaching Assistant,

Rensselaer Polytechnic Institute

APMA 0330-0360: Methods of Applied Math I + II, Teaching Assistant,

Brown University

MATH 0090: Introductory Calculus, Part I; Teaching Assistant, Brown University

Preface and Acknowledgments

To Emma, for believing in me when I did not believe in myself.

To my advisor, Björn Sandstede, for continuing to guide me and work with me through very difficult times.

To my family and friends and everyone else who offered support and encouragement along this journey.

Contents

List of Tables

List of Figures

Chapter

ONE

Introduction

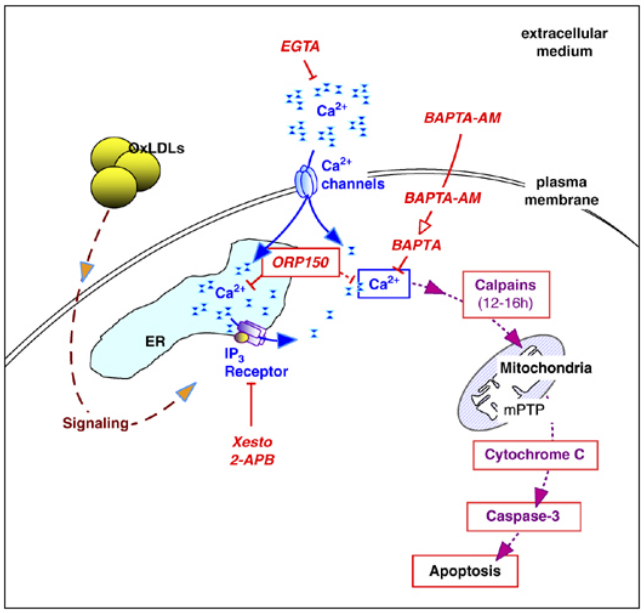

Figure 1.1: Schematic of the role of calcium-induced calcium release in apoptosis. Compare with Figure 1.2. EGTA and BAPTA are examples of buffers (see Section 1.5). Figure recreated from Sanson et al. (2008).

1.1 The biological role of calcium

Calcium is an important second messenger responsible for a variety of cellular and tissue processes including gene expression, cell division and differentiation, apoptosis (Fig. 1.1), and muscle contraction (Fig. 1.2). In this work, we will study in detail models of cellular calcium dynamics. To provide context, however, we will first briefly outline one such process in which calcium is strongly implicated: cardiac excitation-contraction coupling (cardiac muscle contraction). This background will serve to illustrate the biological importance of calcium and help to motivate its study.

In excitation-contraction coupling (Fig. 1.2) an action potential (originating from a motor neuron in skeletal muscle or from the sinoatrial node in the heart) travels through structures in the tissue called T-tubules. The action potential encounters voltage-sensitive calcium channels called L-type calcium channels (LTCC),

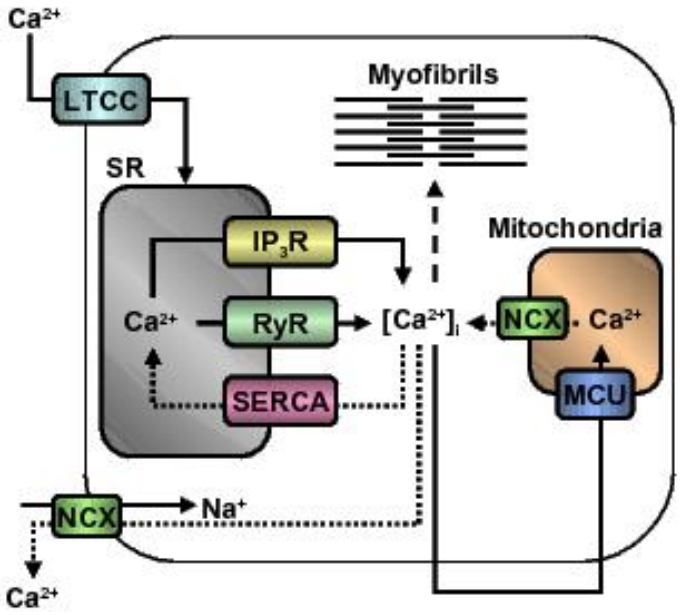

Figure 1.2: Schematic of the role of calcium-induced calcium release in cardiac excitation-contraction coupling. See text for details. Figure recreated from Viola and Hool (2010).

causing them to undergo a conformational change and open, allowing calcium ions to enter the cell cytoplasm. This calcium can then bind to IP_3 receptors (IP_3R) or Ryanodine receptors (RyR) on channels at the surface of the sarcoplasmic reticulum (SR)[1]. The binding of calcium to these channels induces them to open, releasing stores of yet more calcium ions from the interior of the SR into the cytoplasm, significantly amplifying the calcium signal. This process of amplification is called calcium-induced calcium release (CICR) and is the central topic of this thesis.

In muscle tissue, this massive influx of calcium induces contraction of the cell (and thereby, the tissue) via a mechanism called the cross-bridge cycle. Long structures called myofibrils stretch across a muscle cell. These structures are bundles of two different kinds of filaments: thinner filaments comprised of the protein actin, and thicker ones comprised of the protein myosin. Ca^{2+} ions bind to troponin proteins on an actin filament, causing them to undergo a conformational change and

[1]The sarcoplasmic reticulum is a particular kind of endoplasmic reticulum (ER) and the two terms are used interchangeably in the context of calcium-induced calcium release.

expose binding sites on the actin filament. Protrusions on an adjacent myosin filament (called myosin heads) can then attach to these binding sites. The myosin heads attach, pull on the actin filament, detach, and return to their original position. They do this repeatedly in a sort of ratcheting action, causing the actin and myosin filaments to slide against one another. When this occurs in all the myofibrils in the cell, it causes the cell to contract, and when all of the cells in a tissue undergo this process in concert, the tissue contracts. This illustrates the role calcium plays in translating an electrical impulse into the mechanical motion of a muscle tissue. In cardiac tissue, calcium-induced calcium release plays a critical role by amplifying the calcium signal.

A fully quantitative understanding of the mechanisms driving calcium-induced calcium release can therefore provide a more complete understanding of excitation-contraction coupling, and in turn a more complete understanding of cardiac contraction, creating new avenues for medical research and applications.

In this work, we will therefore study individual calcium channels, study the mechanisms that drive their behavior, and examine and improve upon quantitative numerical models of these channels and their behavior.

This chapter will elaborate on the physical process of calcium-induced calcium release, including the importance of individual channels as well as the relevant geometries and dynamics, and will outline the details of the general approach to modeling CICR. Chapter 2 will discuss several approximations and simplifications we have investigated. Chapter 3 will examine the rate constants for channel binding and dissociation reactions, and provide a novel construction of a set of values for these rates determined from experimental data. Finally, Chapter 4 will summarize the results of Chapters 2 and 3, outline the full model as we have constructed it, and discuss further questions not answered by this work.

1.2 Calcium ion channels

In the previous section, we briefly illustrated the biological role of calcium-induced calcium release, and how it is driven by the behavior of individual ion channels: in various kinds of cells, clusters of channels sensitive to inositol 1,4,5-trisphosphate (IP_3) or to Ryanodine are responsible for releasing Ca^{2+} into the cytoplasm from reservoirs in the endoplasmic reticulum (ER). These channels are themselves gated by Ca^{2+}, creating a cooperative phenomenon; the random opening of one channel can encourage other nearby channels to open simultaneously.

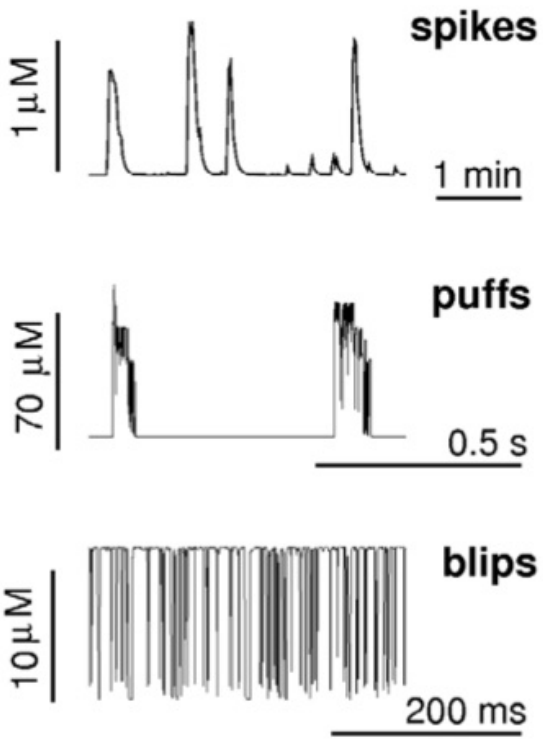

Figure 1.3: A cartoon depiction of different calcium channel events. Figure recreated from (Skupin et al., 2010). Note that blips and puffs are typically measured locally, whereas spikes are averaged over the volume of the cell, creating an apparent discrepancy in the concentration scales.

This cooperativity is significant because it creates a strongly positive feedback process. Not only does this allow for the generation of complex signals, but it means that the termination of CICR must happen at the channel level, further motivating the study of the behavior of individual ion channels.

Because of this cooperative behavior, we observe three types of calcium events (Fig. 1.3): blips - in which a single channel opens and closes repeatedly in rapid succession, puffs - which involve the concerted opening of several channels in one cluster, and spikes (sometimes "sparks") - where several clusters in the cell are ac-

tive simultaneously.

The complexity of these dynamics together with the wide variety of processes that they drive means that CICR is an area of study of significant interest, and many models have been created attempting to explain experimental data. This thesis will discuss recent attempts to model individual calcium channels and clusters thereof. We will discuss in detail several existing approaches to modeling CICR and the assumptions used in these models. We will explore and develop a variety of new approximations and other assumptions and discuss the implications they have for the accuracy and efficiency of the model.

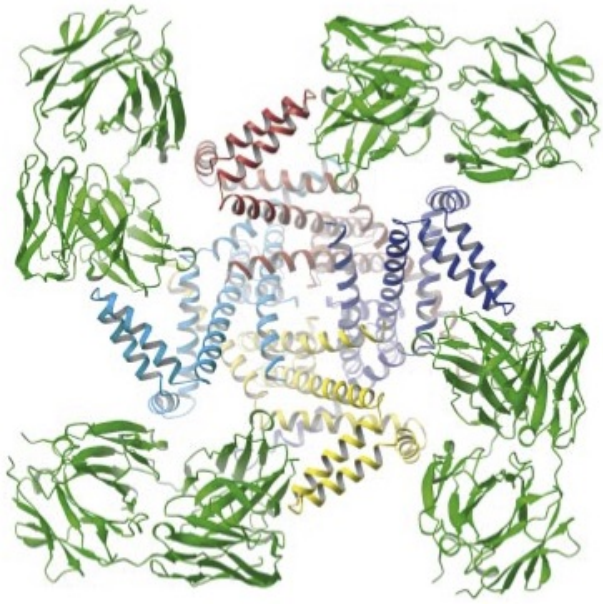

Figure 1.4: 3D model of the protein structure of a voltage-gated potassium channel. Note the four-fold symmetry. Figure recreated from Jiang et al. (2003).

1.3 Channel geometry and dynamics

Imaging of ion channels (Amador et al., 2013, Jiang et al., 2003) (Fig. 1.4) and measurement of single channel currents (Watras et al., 1991) both give evidence suggesting that ion channels possess a tetrameric structure. That is, a channel has four subunits, likely identical and each with independent receptor sites.

IP_3-sensitive calcium channels have been found experimentally to have an open probability distribution that depends strongly on the present Ca^{2+} concentration, exhibiting a bell-like curve (Fig. 1.5). This implies that calcium has both a stimulating and an inhibitory effect on the channel dynamics: when the calcium concentration at a channel is small, the stimulation is weak and the channel does not open often, whereas when the concentration is large, the inhibitory effect is strong and the channel does not open often. Therefore, it is reasonable to assume that each subunit of a calcium channel has three kinds of receptor sites: sites to which IP_3 binds, sites

to which Ca^{2+} binds in such a way so as to encourage activation of the channel, and sites to which Ca^{2+} binds in such a way so as to inhibit activation of the channel.

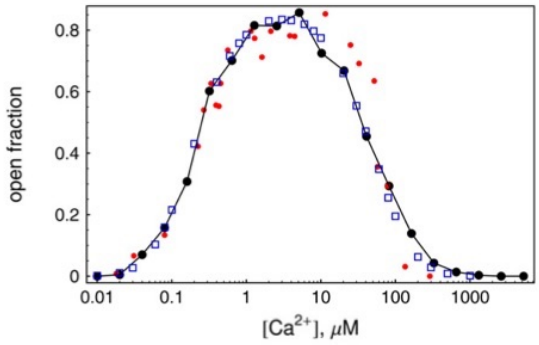

Figure 1.5: The fraction of time a single channel is open as a function of local calcium concentration. Includes both experimental data from (Mak et al., 1998) and simulation results from (Rüdiger et al., 2007). Figure recreated from (Rüdiger et al., 2007).

When a single isolated channel is active, it opens and closes repeatedly in rapid succession, exhibiting a bursting pattern (Swillens et al., 1998, Rüdiger et al., 2007, Dupont et al., 2011, Skupin et al., 2010). These bursts are referred to as blips throughout the literature and typically last around half a second (Rüdiger et al., 2007) with individual openings within a blip lasting around 2-3 ms (Watras et al., 1991, Dupont et al., 2011, Swillens et al., 1998).

Individual channels, however, make up a very small part of the overall picture. While an individual calcium channel has a radius of 6 nm (Skupin et al., 2010, Rüdiger et al., 2007, Dupont et al., 2011, Swillens et al., 1998), a cell measures about 20 μm (Dupont et al., 2011). Additionally, channels group into clusters around 60 nm across (Swillens et al., 1999), which contain about 10-30 channels (Skupin et al., 2010, Swillens et al., 1999) each. The typical distance between clusters in a cell is around 1-3 μm (Dupont et al., 2011, Swillens et al., 1999).

The proximity of channels within a cluster couples their dynamics; one channel opening increases the calcium concentration at nearby channels, which - depending on the exact dynamics - may provoke these other channels to open also. When several channels in one cluster open together in this fashion, it is called a puff. Experimental evidence suggests that puffs typically involve the opening of around five channels (Bootman et al., 1997, Parker and Yao, 1996), and that they actually pre-

dominate in clusters (Sun et al., 1998, Thomas et al., 1998). That is, puff events happen far more frequently than blip events - as many as 95% of cluster events are puffs. Swillens et al. (1999) offer compelling arguments based on these results for the internal geometry of clusters. In particular, neighboring channels in a cluster are likely directly adjacent to one another.

Thus far, we have laid out the biological details of calcium-induced calcium release. The rest of this chapter will be devoted to discussing the general approach to modeling different aspects of the overall problem.

1.4 At the channel: channel stochastics

In the previous sections, we described the internal structure of an ion channel. Specifically, an IP_3-sensitive calcium channel consists of four identical subunits, and each subunit has three different kinds of receptor: IP_3 receptors, activating Ca^{2+} receptors, and inhibiting Ca^{2+} receptors. In this section, we will describe the overall approach to modeling the chemical dynamics of a single channel.

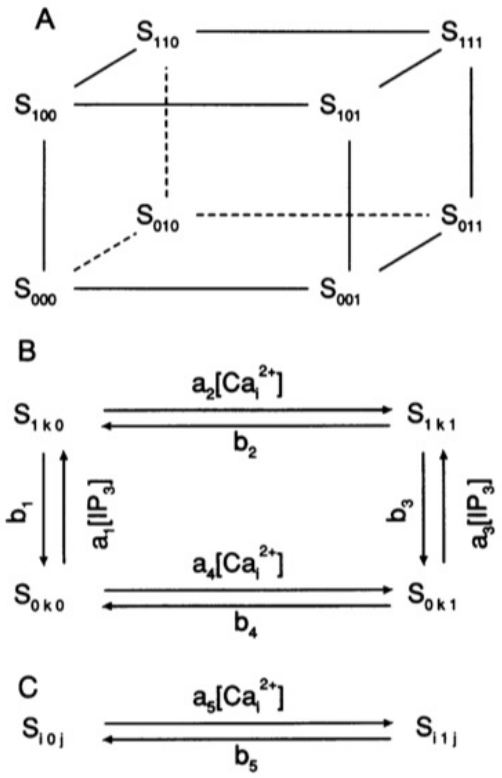

Figure 1.6: The original De Young-Keizer model. The quantities a_j are binding rates and the b_j are dissociation rates (Table 1.1). Figure recreated from (De Young and Keizer, 1992).

A single molecule binding or dissociating from a receptor site can provoke a conformational change for the entire channel, causing it to open or close. Because of this sensitivity, and because of the naturally discrete state space, an obvious way to model channel transitions is as a stochastic process, defining each possible combination of bound receptors as a different state, defining transition rates between them based on the chemical reaction rates for the receptor binding and dissociation, and defining an active subunit state and an opening threshold for the channel: when the number of subunits simultaneously in the active state reaches this threshold, the channel opens and releases calcium. When the number of active subunits falls below this threshold, the channel closes again.

a_1	400	$\mu M^{-1}s^{-1}$	IP_3 binding with no inhibiting Ca^{2+} bound
b_1	52	s^{-1}	IP_3 dissociation with no inhibiting Ca^{2+} bound
a_2	.2	$\mu M^{-1}s^{-1}$	Ca^{2+} binding to inhibiting site with IP_3 bound
b_2	.2098	s^{-1}	Ca^{2+} dissociation from inh. site with IP_3 bound
a_3	400	$\mu M^{-1}s^{-1}$	IP_3 binding with inhibiting Ca^{2+} bound
b_3	377	s^{-1}	IP_3 dissociation with inhibiting Ca^{2+} bound
a_4	.2	$\mu M^{-1}s^{-1}$	Ca^{2+} binding to inhibiting site with no IP_3 bound
b_4	.0289	s^{-1}	Ca^{2+} dissociation from inh. site with no IP_3 bound
a_5	20	$\mu M^{-1}s^{-1}$	Ca^{2+} binding to activating site
b_5	1.65	s^{-1}	Ca^{2+} dissociation from activating site

Table 1.1: Channel transition rates from (De Young and Keizer, 1992). Refer to Figure 1.6 for a schematic illustrating the behavior of channel transitions.

The simplest and most widely used version of this kind of model, introduced by De Young and Keizer (1992), consists of one of each of the three kinds of receptor on each subunit. A subunit is considered to be in an active conformational state when IP_3 is bound and calcium is bound to the activating site but not to the inhibiting site. The channel is considered to be open when at least three of the four subunits are active.

In the De Young-Keizer model, the dynamics for binding and dissociation of molecules at the receptor sites are assumed to be noncooperative between subunits. That is, the rate constants for each binding or dissociation event are dependent only on the local calcium and IP_3 concentrations, and possibly on the current state of the subunit, but not on the states of the other subunits (Fig. 1.6). Specifically, there are eight states in which a subunit can be, and we index these states with a 1 for each molecule if it is bound and a 0 if it is not, in the order IP_3, activating Ca^{2+}, inhibiting Ca^{2+}. For instance, the state S_{110} is the one in which IP_3 is bound and Ca^{2+} is bound to the activating site but not to the inhibiting site, and S_{100} is the state in which only IP_3 is bound.

Statistically, as with any combination reaction, the rate at which binding events occur depends on the number of the binding species present, and so the binding rates

for IP_3 and Ca^{2+} depend on the concentrations of these species near the channel receptors. See Table 1.1 for the values of the rate constants De Young and Keizer used in their model. In Chapter 3, we will examine the choices of rate constants used in different models and elaborate on a method, originally developed by Swillens et al. (1999), for determining the rate constants from experimental data.

1.5 Between channels: reaction-diffusion

The geometry of the cell, and even the internal geometry of a single cluster, is on a much larger scale than the activity of individual calcium ions, and so it is natural to assume a continuum approximation of the calcium ions away from the channels and model the concentration with a standard diffusion equation:

$$\frac{\partial c}{\partial t} = D\nabla^2 c$$

where D is the diffusion constant for calcium and $c = c(\mathbf{r}, t)$ is the calcium concentration at the point $\mathbf{r}$ and at time t.

The boundary conditions for this equation are chosen depending on the scope of the model; a model encompassing the entire cell will necessarily take into account physical conditions at the cell boundary (often either no-flux conditions or a specific flux corresponding to an extracellular signal), whereas a model focusing on a single channel might choose a Dirichlet condition at some arbitrary distance from the channel which is much smaller than the cell length.

We briefly note that it is not immediately clear that a continuum approximation makes sense: if we consider a box whose side length is the diameter of a channel ($R_{ch} = 6$ nm), then a concentration of $[\mathrm{Ca}^{2+}] = .05$ μM corresponds to an average of $5.2 \cdot 10^{-5}$ ions in this box. Additionally, given a channel current of .1 pA and a mean channel open time of 3 ms, every time a channel opens, it releases only about 950 ions. Over the course of a blip event, this number might rise by an order of magnitude. These numbers collectively seem far too small for a continuum approximation to work except far from any channel, where the action of individual ions is unimportant. Nevertheless, the majority of work in the literature uses a continuum approximation, even in the region where a channel is situated.

The most important addition to the diffusion equation is, of course, the influx of calcium when a channel is open. To model this influx, source terms are added to the equation. There are of course many choices for the form of these source terms, but the most common choice is to model them by point sources:

$$\frac{\partial c}{\partial t} = D\nabla^2 c + \sum_j \phi_j(t)\delta(\mathbf{r} - \mathbf{r}_j)$$

where $\mathbf{r}_j$ is the location of the j^{th} channel, δ is the usual Dirac delta,

$$\phi_j(t) = \begin{cases} \phi_0, & j^{th} \text{ channel is open at time } t \\ 0, & j^{th} \text{ channel is closed at time } t \end{cases}$$

and ϕ_0 is the single channel flux strength. In Section 2.4, we will examine and discuss different choices for modeling the source terms.

Other molecules exist naturally in the cytoplasm that can bind to calcium and prevent it from binding to channel receptor sites. These molecules are commonly referred to as "buffers", "ligands", or "chelators" in the literature. The effect of buffers is quantitatively significant for the diffusion of calcium, and so is also typically included in models. Additionally, experiments probing the behavior of calcium channels will often involve adding a dye that binds to calcium ions, allowing the researcher to measure more easily the concentration of calcium in different locations. Thus, in order to be able to compare the result of a model quantitatively to those of an experiment, it is necessary to include the effects of the dye in the model. Naturally-occuring buffers are called endogenous and include mobile buffers which diffuse and stationary buffers which do not. The dye molecules are referred to as dye buffers or exogenous buffers.

Inclusion of these buffers in the model results in additional reaction terms in the equation for c as well as introducing reaction-diffusion equations for each species of

buffer:

$$\begin{aligned}
\frac{\partial c}{\partial t} &= D\nabla^2 c + \sum_{i=s,m,e} \left(k_i^-(B_i - b_i(\mathbf{r},t)) - k_i^+ b_i(\mathbf{r},t)c(\mathbf{r},t)\right) + \sum_j \phi_j(t)\delta(\mathbf{r}-\mathbf{r}_j) \\
\frac{\partial b_s}{\partial t} &= k_s^-(B_s - b_s(\mathbf{r},t)) - k_s^+ b_s(\mathbf{r},t)c(\mathbf{r},t) \\
\frac{\partial b_m}{\partial t} &= D_m\nabla^2 b_m + k_m^-(B_m - b_m(\mathbf{r},t)) - k_m^+ b_m(\mathbf{r},t)c(\mathbf{r},t) \\
\frac{\partial b_e}{\partial t} &= D_e\nabla^2 b_e + k_e^-(B_e - b_e(\mathbf{r},t)) - k_e^+ b_e(\mathbf{r},t)c(\mathbf{r},t)
\end{aligned}$$

where $k_i^{\pm}$ are the reaction rates of the buffers with calcium; B_i is the total concentration of the i^{th} buffer species; b_i is the free (unbound) concentration of the i^{th} buffer species; and the indices s, m, and e refer to the stationary, mobile, and exogenous (dye) buffers, respectively. The total and free concentrations of buffer, B and b, will in general depend on location and time. Generally, the total concentration is much larger than the bound concentration (this also means the free concentration is much larger, and this will help motivate Section 2.3). Additionally, the constant mixing between free and bound buffers means the gradients of total buffer concentrations ought to be much more subtle, even in a region of high activity. Therefore, most models simply take B to be constant.

Since the primary effect of buffers is the slowing of transport of calcium away from an open channel, some models aiming for simplicity will eschew explicit representation of buffers in the model, opting instead for a reduced "effective diffusion" constant for the calcium ions. In Section 2.3, we will examine the strength of the effect of buffers compared to other parts of the model, and explore other simplified methods for the treatment of buffers.

Models aiming for thoroughness may include other terms or even whole equations for other effects. For instance Skupin et al. (2010) use a separate variable E for the lumenal calcium concentration (i.e., that in the ER) which also varies in location and time, and let the current of an open channel depend on the value of $(E - c)$ at the

channel. Skupin's model additionally includes terms modeling pumps transporting calcium back into the ER from the cytoplasm. These effects are beyond the scope of this thesis, but are mentioned here for completeness.

1.6 Coupling the regimes: the Gillespie algorithm

The dynamics of calcium in the cytoplasm and the dynamics of individual molecules and ions binding to receptor sites take place on drastically different spatial and temporal scales. Recall (see Section 1.3), the radius of a channel is 6 nm, while the typical distance between clusters is 1-2 μm, and the cell is about 20 μm across. The mean open time for a single channel (which rapidly opens and closes while bursting) is around 3 ms, while the timescales for whole blips or puffs can easily span hundreds of milliseconds (Rüdiger et al., 2007, Swillens et al., 1999), and larger events (especially spikes) can exhibit behavior on timescales of minutes (Skupin et al., 2010). In contrast, the average time between transitions for a single channel can be as small as 1 ms, and the inclusion of hundreds of channels throughout the cell means transitions throughout the cell are happening on a scale of microseconds. Therefore it makes sense to model the large-scale diffusion and the small-scale channel receptor dynamics separately and find a way to couple the models together.

While diffusion of calcium in the cell can naturally be modeled in a continuum approximation using partial differential equations, each channel is in one of a finite, discrete set of states, and the transitions between states are much better suited to probabilistic modeling.

On the other hand, centering the model on the channel transitions can prove computationally expensive. A naive approach might be to pick a timestep sufficiently small that all channel transitions are rare events, and model it as a traditional Markov chain for a Poisson process. The drawback is that computation of diffusion then has to be done at this timestep, which is much smaller than that needed to model the diffusion accurately.

This motivated the development of a hybrid scheme by Rüdiger et al. (2007) to strike a balance between these two disparate regimes. The goal is to maximize

the amount of simulation time between stochastic computations so that the timestep used to compute diffusion, which is necessarily bounded by the time between stochastic events, may be relaxed. The technique relies on the adapation of an algorithm developed by Gillespie (1977) which consists of drawing two random numbers to determine the properties of the next transition: let α_j denote the transition rates away from the current state of the system, and let $\alpha \equiv \sum_j \alpha_j$. Draw two random numbers $r_1, r_2 \in U(0,1)$. Then the time to the next transition, τ, is given by

$$\tau = \frac{1}{\alpha} \log\left(\frac{1}{r_1}\right)$$

and the index j of the next transition is determined by

$$\frac{1}{\alpha}\sum_{k=1}^{j-1} \alpha_k < r_2 \leq \frac{1}{\alpha}\sum_{k=1}^{j} \alpha_k$$

See Appendix A for a derivation of these formulas.

One will notice that this algorithm creates nonuniform intervals between channel transitions, but this typical transition time is much larger than the timestep of the naive Markov-Poisson model, because each timestep is guaranteed to see precisely one transition instead of having a transition being a rare event. This means that the upper bound the Markov model imposes on the diffusion timestep is much higher, and so a larger diffusion timestep may be chosen with efficiency in mind.

The adaptation by Rüdiger focuses on the fact that, because the channel transitions depend on the local calcium concentration at the channel's receptor sites, and because the calcium concentration is necessarily often in flux, the transition rates themselves are not constant in time. In other words, Gillespie's algorithm assumes that all of the transition rates are constants, while Rüdiger's implementation extends the algorithm to time-dependent rates as follows: let $\alpha_j = \alpha_j(t, c(t))$ and let $\alpha = \alpha(t, c(t))$ be defined analogously as before. Then the time to next transition is

given by (see Appendix A for details)

$$\int_0^\tau \alpha(t', c(t'))dt' = \log\left(\frac{1}{r_1}\right)$$

Note that, in the event that α is constant, this equation reduces precisely to $\tau = \frac{1}{\alpha}\log\left(\frac{1}{r_1}\right)$. If we define $g(t) = \int_0^t \alpha(t', c(t'))dt'$, this suggests the following initial value problem:

$$\frac{dg}{dt} = \alpha(t, c(t)); \qquad g(0) = 0$$

which can be evolved numerically until g reaches the value $\log\left(\frac{1}{r_1}\right)$. Since $\alpha_j > 0$, a solution $g(\tau) = \log\left(\frac{1}{r_1}\right)$ is guaranteed to be unique. Existence of a solution is not mathematically guaranteed for every set of α_j, but such situations are decidedly unphysical. In particular, in the context of modeling calcium dynamics, such a situation would require all of the IP_3 and Ca^{2+} to leave the cell cytoplasm. Thus, Gillespie's algorithm may still be applied, in Rüdiger's form, to the problem of modeling calcium ion channel dynamics, allowing the optimization of the stochastic timestep.

1.7 Summary

In this chapter, we have outlined the biological phenomenon of calcium-induced calcium release as well as the general approaches to modeling diffusion of calcium away from channels and modeling channel receptor reactions. We have also discussed a method for coupling together these two regimes in a precise way.

In the next two chapters, we will delve more deeply into the details of employing these modeling approaches and examine different choices that may be made, along with their advantages and drawbacks. We will also examine some approximations that can be made to simplify the model and reduce computation time, and discuss the relative impact of these approximations on the accuracy of the overall model.

The purpose of our work was to streamline existing approaches to modeling CICR, that is, to improve the overall accuracy and efficiency by examining different modeling approaches. The specific results we found are as follows:

- The assumption that the calcium concentration immediately equilibrates to a steady-state spatial profile upon the opening or closing of a single channel is a useful and reasonable approximation.
- The assumption that the concentrations of any buffer species do not depend on location or time is a useful and reasonable approximation.
- It is possible to model CICR treating a cluster as a single, fundamental stochastic object and obtain qualitatively reasonable results.
- The assumption that the single-channel flux is concentrated at a point is not a reasonable approximation and is of questionable usefulness. Instead, taking the flux to be uniform over the channel volume offers an approach with less

arbitrariness that is neither computationally expensive nor difficult to implement.

- It is possible to construct channel receptor binding and dissociation rates for a cluster of channels using data from experimental results. The use of such a construction yields a working numerical model for a cluster of calcium channels.

The first three results are significant for their implications towards model efficiency; these simplifications dramatically reduce computation time and at least the first two do so without significantly impacting the accuracy of the model. The fourth result is important due to its ubiquity in the literature. We examine the drawbacks to this approach and offer an easy alternative. Finally, the last result is, to our knowledge, a novel result that may allow for more careful analysis of the inner workings of calcium channel binding reactions as well as ultimately provide the means for more exact quantitative models of CICR.

Chapter

TWO

Approximations

2.1 Overview

With any computation of sufficient complexity, a choice must be made in how to strike a balance between thoroughness and computational tractability. Many models in the literature focus on examining a single cluster of calcium channels or just one isolated channel. These problems involve sufficiently few quantities that a fully accurate model is not very computationally expensive. However, when one considers an entire cell with as many as 50 clusters, the cost goes up dramatically: diffusion occurs on a much wider domain but must still be treated with sufficiently fine granularity to account for the internal geometry of a cluster, the spherical symmetry used to model diffusion is lost, the number of possible transitions increases tremendously, and the expected time between channel transitions becomes one or two orders of magnitude smaller.

Computational techniques exist to mitigate these problems to a degree. Nevertheless, models examining an entire cell typically require the use of a supercomputer to become manageable. One of the primary aims of this thesis is to examine approximations and simplifications that can dramatically reduce the computational time for a full-cell model while keeping sufficient accuracy to provide at least qualitatively useful results.

In this chapter, we will discuss timescales of different parts of the model, the relative impact of buffer dynamics, several simplifications involving the limiting solution of an open channel, and the relationship between single channel statistics and cluster statistics. In particular, we will examine the following approximations:

- the assumption that the effect of channel influx occurs instantaneously
- the assumption that the buffer concentrations are independent of location and time

- the assumption that the flux due to an open channel is concentrated at a point
- a simplification wherein puffs, instead of blips, are the fundamental stochastic event and individual channel behavior is not explicitly computed

We will demonstrate that the first two assumptions are good approximations, that the third is not, and that the fourth is plausible.

2.2 Instantaneous equilibration

2.2.1 Motivation

When recreating existing models, it quickly became apparent that the computations required to calculate the diffusion of calcium ions dwarfed those for the channel transitions in terms of number of computations per timestep. This proved to be true regardless of the approach used in computing the diffusion. Skupin et al. (2010) approached the problem by using Green's functions in order to be able to compute the calcium concentrations only locally at each channel location instead of everywhere on a large mesh. However, because of the geometry of the problem, the Green's functions involved infinite series of eigenfunctions, the approximation of which still left many terms to be computed and proved to be computationally expensive. Skupin et al. made explicit mention of the use of a supercomputer to analyze their model.

It seemed apparent that the most dramatic way to speed up the computation time was to find a way to eschew the diffusion computation altogether. When modeling a single calcium channel, we noticed that the calcium concentration increased rapidly near a channel upon opening and quickly leveled off. Additionally, this profile had limited spatial extent; beyond a certain distance - only a fraction of the cell radius - the difference between $c(r)$ and the base cytosolic concentration c_0 was a very small fraction of c_0.

In models with relatively high buffer concentrations, we even found that everywhere in the cell, the spatial calcium profile approached a steady state, and that after a fraction of the cell radius, the spatial profile dropped to within machine error of c_0.

A single channel opening or closing therefore had a very rapid effect on an intracluster scale and a very weak effect on an intercluster scale. Thus, we examined

the possibility of assuming that a channel instantaneously achieves this steady-state profile upon opening, and that the profile instantaneously decays back to c_0 upon closure of the channel.

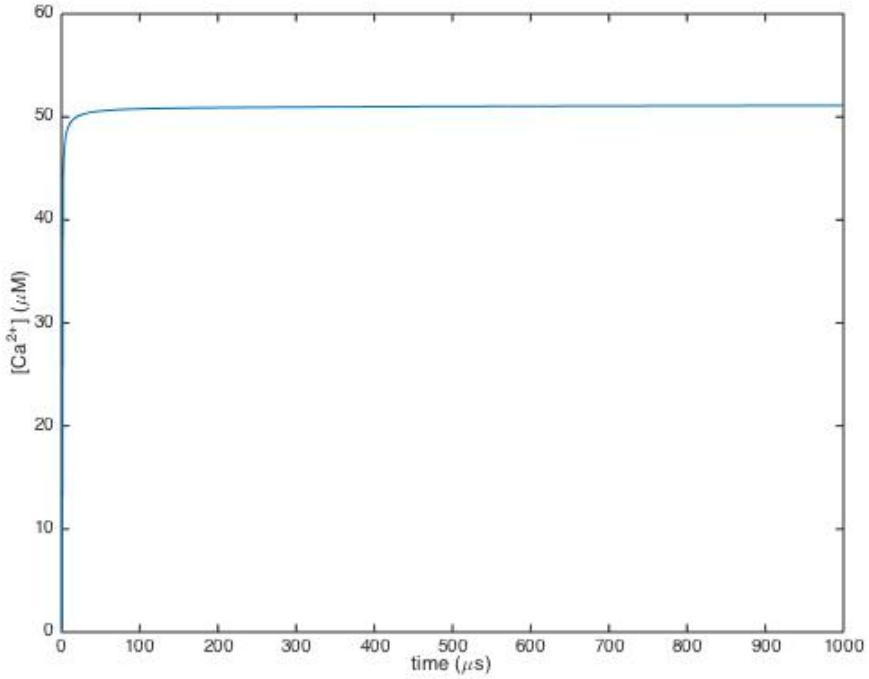

Figure 2.1: Time evolution of the calcium concentration at an open channel with no approximations. Biological parameters used are from (Rüdiger et al., 2007). Modeled using a finite-difference scheme with the full reaction-diffusion equations for c and b_i with three species of buffer. Channel flux distribution uniform over the channel volume.

2.2.2 Fast timescale of channel influx

The three possible mechanisms for closing a channel are: 1. dissociation of IP_3 from an active subunit, 2. dissociation of Ca^{2+} from the activating site of an active subunit, and 3. binding of Ca^{2+} to the inhibiting site of an active subunit. Since three active subunits are required for a channel to be open, the average closing rate will then be roughly three times the sum of the rates for these three events. With the nomenclature of Table 1.1, the closing rate will be $3 \cdot (b_1 + b_5 + a_2 c)$ and the average time to close will be the reciprocal of this quantity. Looking at the parameters from Table 2.1, and taking an at-channel peak concentration of 50 μM, the fastest average

closing time possible is roughly $t_{\text{close}} = \frac{1}{500\ \text{s}^{-1}} = 2$ ms, which also matches well the observed mean open time for a single channel (Section 1.3).

Thus, if the concentration at the channel levels off or even slows substantially in much less than a millisecond, a channel that has just opened is extremely unlikely to undergo a state transition before the local concentration reaches this plateau. Thus for the purposes of computing channel transitions, it would be a good approximation to assume the concentration reaches this level instantaneously, as doing so would make no difference to the channel's dynamics. We found such a rapid leveling off to be the case for a variety of sets of biological parameters and stochastic transition rates.

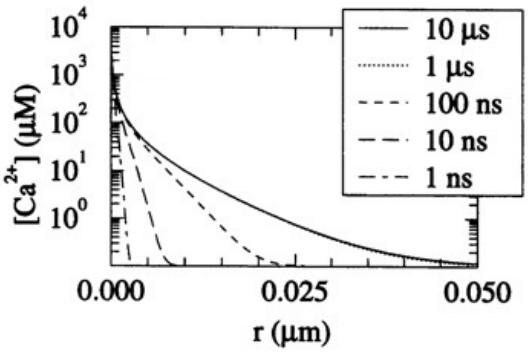

Figure 2.2: Time evolution of the spatial calcium concentration profile. Recreated from (Smith et al., 1996). Of particular note is the 10 mM exogenous buffer concentration.

In Figure 2.1, we have shown this leveling off for a model consisting of a single channel in the center of a cell-sized sphere with Dirichlet boundaries, giving a full dynamical treatment of the buffers. It is evident that in this case, the concentration doesn't quite reach an equilibrium value within the first millisecond. Nevertheless, it increases extremely rapidly for the first 50 microseconds or so, and then for the rest of that first millisecond, rises extremely slowly. In situations where the model includes a large buffer concentration or ignores the dynamics of the buffers and takes them to be constant (an approximation that will be explored in depth in Section 2.3), the situation is even more dramatic. In both cases, the spatial concentration profile quickly reaches a steady-state distribution. In the former case (Fig. 2.2), the entire profile equilibrates within 1 µs. In the latter (Fig. 2.3), the entire profile equilibrates within .6 ms, and the at-channel concentration equilibrates within .1 ms. In any case, the

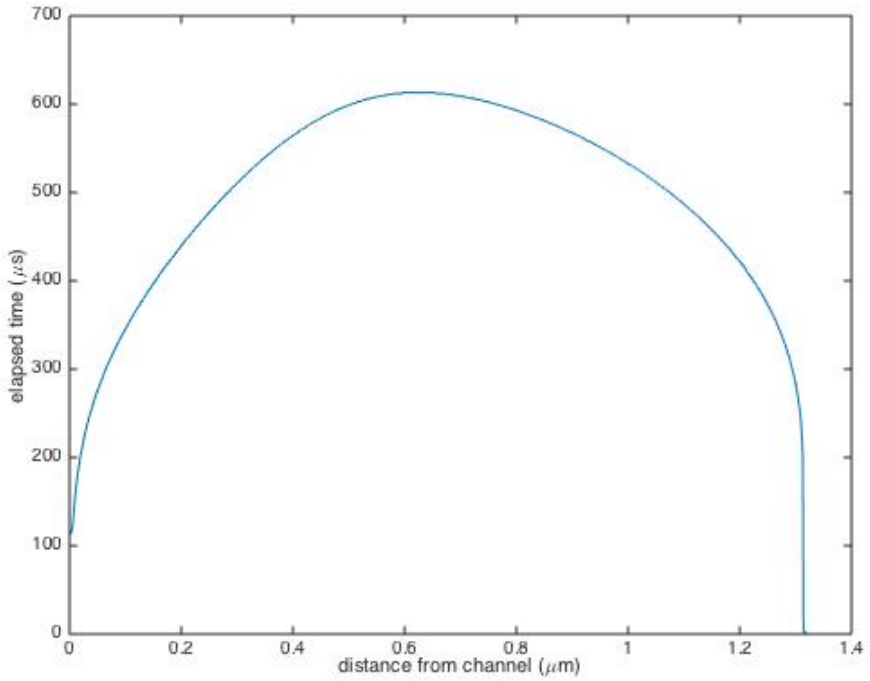

Figure 2.3: Time for the concentration at a point to reach 99.9% of the equilibrium concentration at that point. All model parameters are the same as in Figure 2.1 except the buffer species concentrations are treated as constant - both uniform throughout the cell and independent of time. The reason the time falls to 0 at around 1.3 μm is because c_0 is already within 99.9% of the equilibrium value. Beyond this point, the effect of the channel is negligible.

effect of an open channel on itself can justifiably be assumed to be instantaneous with respect to the receptor binding reactions.

	(a)	(b)	(c)	(d)		(e)
a_1	20	400	80	20	k_i^+	35.8
b_1	20	52	.64	52	k_i^-	5
a_2	.001	.2	.04	.001	k_d^+	.088
b_2	.03	.2098	.48	$3.077{\cdot}10^{-4}$	k_d^-	1.67
a_3	2.6	400	80	20	k_i^+	35.8
b_3	20	377	40	52	k_i^-	5
a_4	.025	.2	.4	.025	k_d^+	.088
b_4	.1	.0289	.0768	.0025	k_d^-	1.67
a_5	10	20	15	10	k_a^+	166
b_5	1.225	1.647	12	122.5	k_a^-	65.9

Table 2.1: Comparison of channel rate constants from various models. Units are $\mu M^{-1}s^{-1}$ for binding rates (a_i) and s^{-1} for dissociation rates (b_i). Repeated and elaborated upon in Chapter 3 (Table 3.2).

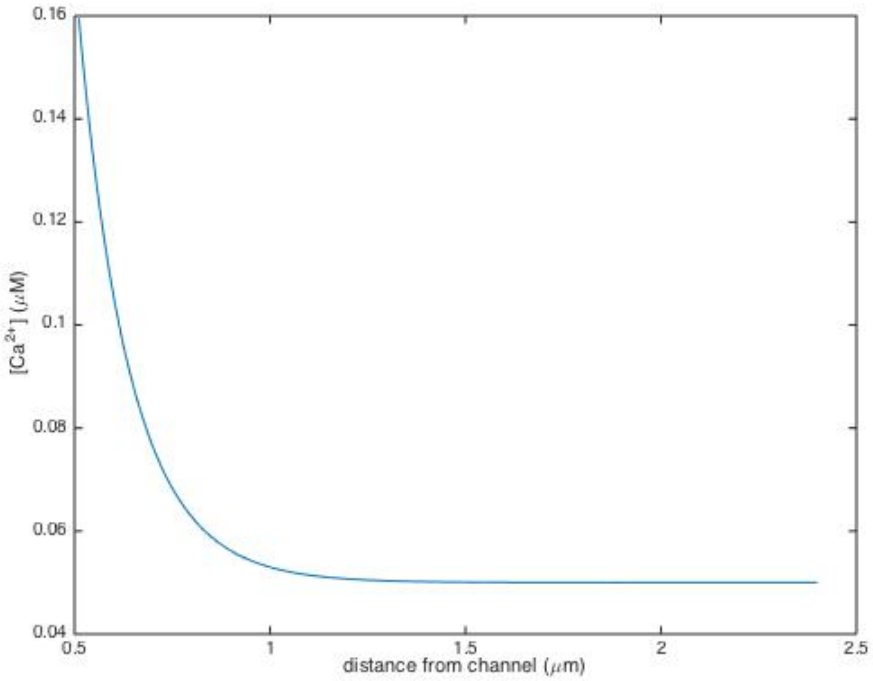

Figure 2.4: Spatial distribution of calcium due to a cluster with five open channels 2.5 ms after opening.

2.2.3 Limited spatial extent of channel influx

In the previous section, we illustrated that a channel opening has an extremely rapid effect in its vicinity. We also touched on the fact that, although the effect of an open channel is felt more slowly far from the channel, that effect is much smaller. In this section, we will briefly illustrate this fact.

The typical distance between clusters is 1-2 μm. We modeled the effect of a source five times as strong as an individual channel (Fig. 2.4) and found that even after a couple milliseconds had elapsed, the effect of the active cluster had only just reached 1 μm. Even at half this distance, the elevated concentration was only about three times the base level - a fraction of the effect of a channel on its neighbors.

In fact, if we include the approximation of treating buffers as constant, the spa-

tial profile achieves within a couple milliseconds a steady-state profile that does not change to within machine error. This profile drops to within 0.1% of c_0 at 1.3 μm from the cluster (Fig. 2.3), and to within machine error of c_0 at about 4 μm from the cluster - only 20% of the cell diameter.

In the previous section, we demonstrated that the effect of an open channel on itself and its neighbors propagates on a timescale much shorter than the typical stochastic transition time, and so near an open channel, the calcium concentration profile may be assumed to take effect instantaneously. Here, we have shown that the effect of an open channel outside of its home cluster is so small that making this assumption will not have a profound effect on the dynamics of other clusters. We have therefore justified that taking this approximation for a full-cell model is reasonable.

2.2.4 Eliminating time evolution from the diffusion computation

We have just demonstrated that assuming instantaneous equilibration of the concentration profile upon a channel opening is a reasonable approximation to make. The obvious implication is that continuous time evolution is no longer needed for modeling the diffusion of calcium through the cell. In this section, we illustrate how this leads to a very simple computation of the calcium concentration at any point in the cell.

Recall the reaction-diffusion equations for c and b:

$$\begin{aligned}
\frac{\partial c}{\partial t} &= D\nabla^2 c + \sum_{i=s,m,e} \left(k_i^-(B_i - b_i(\mathbf{r},t)) - k_i^+ b_i(\mathbf{r},t)c(\mathbf{r},t)\right) + \sum_j \phi_j(\mathbf{r},t) \\
\frac{\partial b_s}{\partial t} &= k_s^-(B_s - b_s(\mathbf{r},t)) - k_s^+ b_s(\mathbf{r},t)c(\mathbf{r},t) \\
\frac{\partial b_m}{\partial t} &= D_m\nabla^2 b_m + k_m^-(B_m - b_m(\mathbf{r},t)) - k_m^+ b_m(\mathbf{r},t)c(\mathbf{r},t) \\
\frac{\partial b_e}{\partial t} &= D_e\nabla^2 b_e + k_e^-(B_e - b_e(\mathbf{r},t)) - k_e^+ b_e(\mathbf{r},t)c(\mathbf{r},t)
\end{aligned}$$

The first equation is affine in c and we can exploit this fact in combination with instantaneous equilibration to make computation of the calcium concentration at any point in the cell quite easy.

Suppose we have two steady-state solutions $c_{1,2}(\mathbf{r})$ corresponding to open channels at two distinct locations $\mathbf{r}_{1,2}$. For simplicity, assume only one buffer species. Then c_j satisfies:

$$D\nabla^2 c_j - k^+ b(\mathbf{r})c_j(\mathbf{r}) + k^-(B - b(\mathbf{r})) + \phi(\mathbf{r} - \mathbf{r}_j) = 0$$

This equation has a constant solution $c_0 = K\frac{B-b_0}{b_0}$ when all channels are closed (see Appendix B for more details). Let $c_j(\mathbf{r}) \equiv c_0 + f_j(\mathbf{r})$. Then the equation reduces to

$$D\nabla^2 f_j - k^+ b(\mathbf{r}) f_j(\mathbf{r}) + \phi(\mathbf{r} - \mathbf{r}_j) = 0$$

So $f \equiv f_1 + f_2$ satisfies

$$D\nabla^2 f - k^+ b(\mathbf{r}) f(\mathbf{r}) + \phi(\mathbf{r} - \mathbf{r}_1) + \phi(\mathbf{r} - \mathbf{r}_2) = 0$$

and so $c \equiv c_0 + f_1 + f_2 = c_0 + (c_1(\mathbf{r}) - c_0) + (c_2(\mathbf{r}) - c_0)$ satisfies

$$D\nabla^2 c - k^+ b(\mathbf{r}) c(\mathbf{r}) + k^-(B - b(\mathbf{r})) + \phi(\mathbf{r} - \mathbf{r}_1) + \phi(\mathbf{r} - \mathbf{r}_2) = 0$$

which is the full time-independent equation for two open channels.

There is a subtlety here, which is that c_1 and c_2 actually satisfy equations with different functions $b(\mathbf{r})$ (recall, however, that we assume from the start that B is constant). Neher (1986) demonstrates that the maximal change in buffer concentration due to an open channel is quite small compared to the total buffer concentration, and so takes the buffer concentration to be uniform (an approximation that will be looked at more closely in the following section). This assumption implies the above result.

If c_1 and c_2 satisfy either $c_j = c_0$ or $\frac{\partial c_j}{\partial n}$ at the cell boundary (which are the two most realistic scenarios), then clearly so will c, and so c is also a solution of the full boundary-value problem.

More generally, this means that if $c_k(\mathbf{r})$ is the steady-state solution for the k^{th} channel (which may, in general, depend on the geometry of the cell), then the full

steady-state solution for an arbitrary number of channels N is given by

$$c(\mathbf{r}) = c_0 + \sum_{k=1}^{N} (c_k(\mathbf{r}) - c_0) \cdot o_k$$

where

$$o_k = \begin{cases} 1, & k^{th} \text{ channel is open} \\ 0, & k^{th} \text{ channel is closed} \end{cases}$$

which is trivial to implement numerically.

If we assume instantaneous equilibration as detailed earlier in this chapter, then we can allow the o_k to depend on time, and the full time-dependent solution for the problem becomes

$$c(\mathbf{r}, t) = c_0 + \sum_{k=1}^{N} (c_k(\mathbf{r}) - c_0) \cdot o_k(t) \tag{2.2.1}$$

In other words, assuming instantaneous equilibration allows us to reduce solving the PDE to what amounts to a single inner product of two vectors, one of which does not depend on time and can be precomputed solely from considerations of geometry.

2.2.5 Handling the geometry

With the use of equation 2.2.1, the time evolution of diffusion is completely removed from the computational process, and the only aspect of solving the reaction-diffusion equation that remains is examining the interaction between the sources and the cell boundary. We examine a few easy choices.

If we assume Dirichlet conditions at the cell boundary, then this formula is very easy to implement generally over the whole domain of the cell. A spherical domain with a constant value on the boundary has a simple solution using the method of images: for each channel in the cell, we can create a corresponding image source outside the cell with an appropriately scaled strength. The drawback to this method is that a Dirichlet condition on the cell boundary is unphysical and likely to be a poor approximation to a real biological situation.

A Neumann boundary condition is much more physically appropriate, and can still be treated using the method of images, but spherical symmetry doesn't allow for such a simple, elegant solution to this problem. Instead, the solution yields a Green's function consisting of an infinite series of terms, much like that used by Skupin et al. (2010), and so any computational efficiency gained from employing the instantaneous equilibration assumption is lost again in approximating this series.

As demonstrated in Section 2.2.3, the single-channel steady-state profile has a finite extent depending on the biological parameters chosen for the model; using the set of biological parameters from (Rüdiger et al., 2007) and treating the buffer concentrations as constant, we had $c(r) - c_0 < \epsilon_{mach}$ for $r > .35\, R_{cell}$. This lends itself to another possible approximation for the full cell geometry, namely restricting the possible locations of the channels to a region in the center of the cell this distance from the cell boundary. This situation is further justified by the possibility of IP_3-sensitive channels being localized in a region roughly 6 μm wide (Callamaras and

Parker, 1999) while the cell is roughly 20 μm across. In this case, the effects of any open channel therefore never make it as far as the cell boundary, and we can use the simplified formula for $c(\mathbf{r}, t)$ everywhere in the cell without worrying about the boundary condition; both a constant boundary condition and a no-flux boundary condition are automatically satisfied to within machine error.

In this case, if we take instantaneous equilibration of channel dynamics as an assumption, then the full solution to the reaction-diffusion equation for c becomes

$$c(\mathbf{r}, t) = c_0 + \sum_{k=1}^{N} (\tilde{c}(\mathbf{r} - \mathbf{r}_k) - c_0) \cdot o_k(t)$$

where $\tilde{c}$ is the steady-state solution for a single channel at the origin and $\mathbf{r}_k$ is the location of the k^{th} channel. That is, only one steady-state distribution needs to be computed in this case, along with the set of pairwise distances between channels. This is clearly a remarkably simple and computationally inexpensive method to implement in a numerical model.

2.2.6 The Gillespie-Rüdiger algorithm

In the last section, we described how the assumption that an open channel instantaneously reaches a steady-state spatial distribution, along with the assumption of either of two realistic boundary conditions, leads to a remarkable simplification of the computation of diffusion of calcium throughout the cell. While this is likely the most dramatic impact of this approximation - because the computation of diffusion is the most computationally expensive part of the model - it is not the only one.

Recall the Gillespie-Rüdiger algorithm for computing the stochastic transitions: given stochastic transition rates $\alpha_k(t)$ with $\alpha(t) \equiv \sum_k \alpha_k(t)$, we may compute the time of the next transition, τ, by evolving

$$\frac{dg}{dt} = \alpha(t, c(t)); \qquad g(0) = 0$$

until $g(\tau) = \log\left(\frac{1}{r}\right)$ where r is a random number selected uniformly from $(0, 1)$. (See Section 1.6 for an overview of the algorithm or Appendix A for details.)

Following this algorithm therefore requires numerically evolving an ODE at every stochastic timestep. However, if we use the approximation of instantaneous equilibration, the transition rates α_k no longer depend on time. Between transitions, they are all constant since c is independent of time. Therefore, the computation of τ reduces to the original version given by Gillespie:

$$\tau = \frac{1}{\alpha} \log\left(\frac{1}{r}\right)$$

Thus, the numerical evolution of an ODE is replaced by a very small number of operations.

2.3 Constant buffers

2.3.1 Motivation

Recall the full reaction diffusion system:

$$\begin{aligned}
\frac{\partial c}{\partial t} &= D\nabla^2 c + \sum_{i=s,m,e} \left(k_i^-(B_i - b_i(\mathbf{r},t)) - k_i^+ b_i(\mathbf{r},t)c(\mathbf{r},t)\right) + \sum_j \phi_j(\mathbf{r},t) \\
\frac{\partial b_s}{\partial t} &= k_s^-(B_s - b_s(\mathbf{r},t)) - k_s^+ b_s(\mathbf{r},t)c(\mathbf{r},t) \\
\frac{\partial b_m}{\partial t} &= D_m\nabla^2 b_m + k_m^-(B_m - b_m(\mathbf{r},t)) - k_m^+ b_m(\mathbf{r},t)c(\mathbf{r},t) \\
\frac{\partial b_e}{\partial t} &= D_e\nabla^2 b_e + k_e^-(B_e - b_e(\mathbf{r},t)) - k_e^+ b_e(\mathbf{r},t)c(\mathbf{r},t)
\end{aligned}$$

Here, there are four (or more, if more than one species of each kind of buffer is modeled) separate quantities to compute, and the computational cost of diffusion - which is already the most expensive part of modeling CICR - scales with the number of these quantities. Being able to reduce this system to one equation would therefore have a positive impact on the computational cost of the model, and because the calcium concentration is the principle quantity of interest, the simplest way of doing this is simply to ignore the other three equations and model the unbound buffer concentrations as uniform throughout the cell and constant in time (recall that the total buffer concentrations are already assumed to be thus).

Additionally, as alluded to in the previous section, this assumption of constant buffers couples nicely with the assumption of instantaneous equilibrium, making the implementation and justification of the latter significantly easier. In particular, with the assumption of constant buffers, the time evolution of the spatial calcium profile due to influx of an open channel not only slows rapidly, but in fact reaches a steady-state distribution on a timescale that is on the same order of magnitude as

the average stochastic transition time for a single channel.

Using the assumption of constant buffers allows us to model a single channel with any set of parameters and any source distribution desired, quickly compute the steady-state distribution, and use that distribution throughout the rest of the model.

The primary impact of buffers is twofold: altering the diffusion dynamics of the calcium concentration, and affecting the equilibration speed at an open channel. In the next section, we will demonstrate that the assumption of constant buffers does not significantly influence either of these effects, and that it is therefore a reasonable assumption to make.

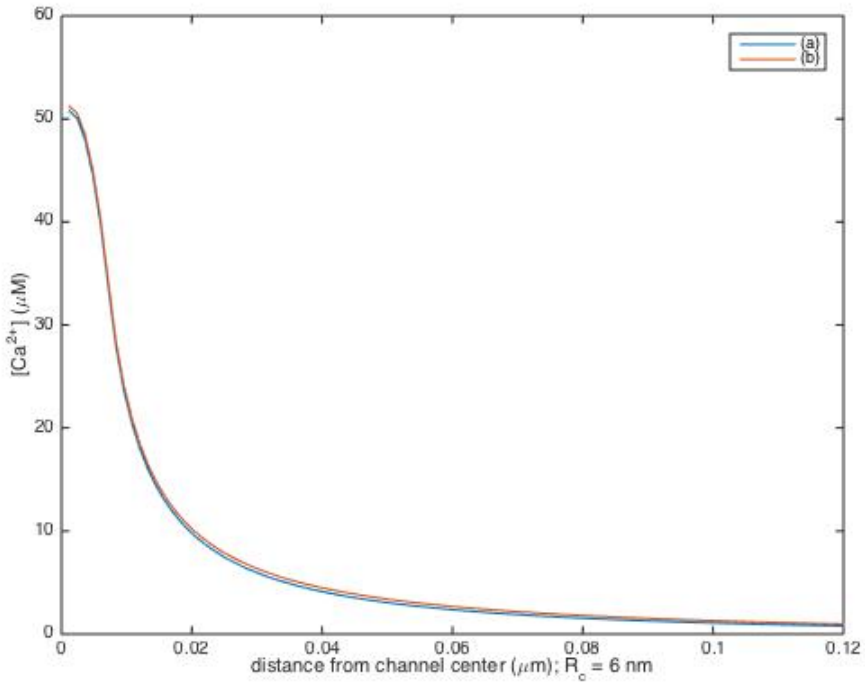

Figure 2.5: Comparison of the spatial profiles due to the influx of a single channel with (a) constant and (b) dynamically evolved buffers. Elapsed time is 2.5 ms. Biological parameters from Rüdiger et al. (2007), with uniform flux over channel volume. Computed with 2nd-order radially symmetric finite difference scheme and 4th-order Runge-Kutta method. Dirichlet conditions at cell boundary. See Figure 2.6 for a plot of the absolute error.

2.3.2 Justification

The primary effect of buffers is on the diffusion dynamics of calcium. In Sections 2.2.2 and 2.2.3, we illustrated that there are effectively two regimes for diffusion: far from a channel, where the effect of influx due to an open channel is felt slowly but weakly, and near the channel, where this effect is felt strongly but rapidly. In this section, we will demonstrate that the assumption of constant buffers preserves the weakness of the former and rapidity of the latter.

Figures 2.5 and 2.6 compare the results of modeling a single channel with constant or dynamic buffers. The elapsed time in both cases is 2.5 ms, which (see

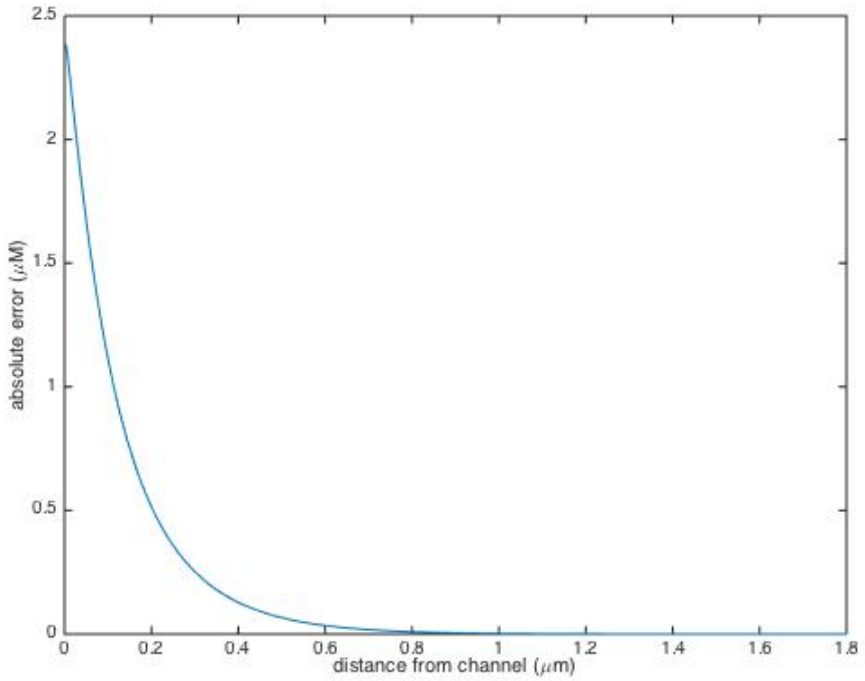

Figure 2.6: The absolute error corresponding to Figure 2.5. The error is small compared to $c_0 = .05$ μM far from the channel.

Section 1.3) is roughly equal to the expected open time for the channel. Therefore, even though, should the channel remain open, the dynamic-buffer profile would continue to rise (Fig. 2.1), the channel is unlikely to remain open much longer than this amount of time. These results show that far from an open channel, the effect of the constant buffer approximation is negligible and preserves the weakness of the open channel's effect at these distances.

Next, we will examine the effect of this assumption at the channel itself. Suppose that the buffer concentrations are indeed constant, and for simplicity, assume only one buffer species. Additionally, consider a situation with only one channel. The reaction diffusion equation for calcium is then

$$\frac{\partial c}{\partial t} = D\nabla^2 c - k^+ bc(\mathbf{r}) + k^-(B - b) + \phi(\mathbf{r} - \mathbf{r}_j)$$

When the channel is closed, there is a constant solution $c_0 = K\frac{B-b}{b}$, and when the channel is open, assume there is a steady-state solution $c(\mathbf{r}) = c_0 + \tilde{c}(\mathbf{r})$ with $\tilde{c}$ satisfying

$$D\nabla^2\tilde{c} - k^+ b\tilde{c}(\mathbf{r}) + \phi(\mathbf{r} - \mathbf{r}_j) = 0$$

The steady-state solution in the case that ϕ is a point source is derived in Appendix B. Then the full time-dependent solution when the channel is closed is given by

$$c_{\text{closed}} \;=\; c_0 \;+\; F(\mathbf{r}, t)$$

and the solution when the channel is open is given by

$$c_{\text{open}} = c_0 + \tilde{c}(\mathbf{r}) + G(\mathbf{r}, t)$$

where F and G both satisfy

$$\frac{\partial F}{\partial t} = D\nabla^2 F - k^+ bF$$

This equation is separable: let $F(\mathbf{r}, t) = R(\mathbf{r})T(t)$. Then we have:

$$\frac{1}{T}\frac{dT}{dt} = \frac{1}{R}\left(D\nabla^2 R - k^+ bR\right) \equiv -\nu$$

The equation for T yields $T(t) = e^{-\nu t}$ and so ν is going to be a characteristic decay rate for a particular mode. The modes are determined by

$$D\nabla^2 R + (\nu - k^+ b)R = 0$$

along with boundary or regularity conditions. This equation will only have solutions that are regular over the whole domain when $\nu - k^+ b \geq 0$ and so the smallest possible

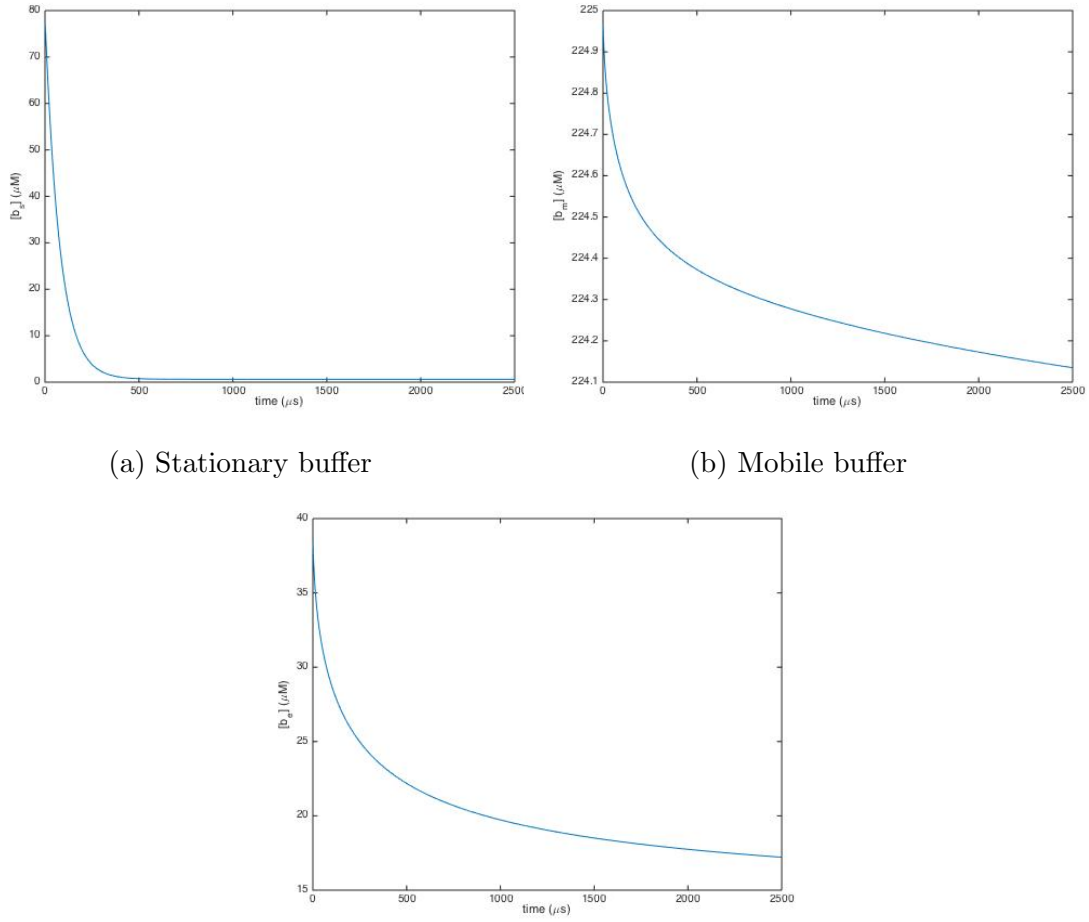

(a) Stationary buffer

(b) Mobile buffer

(c) Exogenous buffer

Figure 2.7: The time evolution of the buffer species concentrations at an open channel. Total elapsed time 2.5 ms.

value of ν is given by $\nu_0 = k^+ b$. Since ν represents a decay rate, the smallest value will represent the slowest decay mode, and thus represent the overall equilibration rate of the solution. In particular, it should be the case that $\frac{1}{\nu_0}$ gives the characteristic equilibration time.

Generalizing to several buffer species, it is easy to see that

$$\nu = \sum_j k_j^+ b_j$$

and so we may verify this result using, for instance, the biological parameters from (Rüdiger et al., 2007). In this case, we have $b_s = 78$ μM, $b_m = 225$ μM, $b_e = 39$ μM, $k_s^+ = 50$ $\mu M^{-1}s^{-1}$, $k_m^+ = 5$ $\mu M^{-1}s^{-1}$, and $k_e^+ = 150$ $\mu M^{-1}s^{-1}$. Therefore, $\nu_0 = 11000$ s^{-1} and $\frac{1}{\nu_0} = 92$ μs, which matches closely the results seen in Figure 2.1.

This computation has been performed assuming that the buffers are constant. Removing this assumption, an analytic examination of the decay modes is not so easy, but it should be the case that in a small time interval, the decay rate in that interval is approximately what it would be retaining this formula for ν_0.

Allowing the concentrations to evolve numerically for 2.5 ms, using the same model as in Figure 2.5 (with dynamic buffers), we find (Fig. 2.7) the buffer concentrations to be $b_s = .6$ μM, $b_m = 224$ μM, and $b_e = 17$ μM after this amount of time. Using these values, we find $\frac{1}{\nu_0}$ to be 270 μs. This is three times as large as the value obtained using constant buffers, but is still small compared to the mean open time of 2 ms.

The assumption of constant buffers, therefore, not only gives a result consistent with the numerical results from a simulation with no approximations (Fig. 2.1), but gives a result that is robust upon removal of the assumption.

We have therefore shown that assuming the buffer concentrations are constant is a good approximation both near an open channel and far away from it.

2.4 Channel flux distribution

2.4.1 Motivation

Because of the self-affecting nature of calcium ion channels, it is important to be able to accurately model the effect of an open channel on itself. Furthermore, the influx from an open channel creates a strong concentration gradient (Fig. 2.5), and so the effect of an open channel on itself is much greater than the effect even on directly adjacent channels. Therefore, it is critical to be able to model the concentration at an open channel accurately.

Much of the literature (e.g., Skupin et al. (2010), Swillens et al. (1998)) chooses to model the influx of calcium using a point source. That is,

$$\phi(\mathbf{r}) = \phi_0 \cdot \delta^3(\mathbf{r})$$

where ϕ_0 is a constant characterizing the flux strength and $\delta^3(\mathbf{r})$ is the usual three-dimensional Dirac delta.

In this section we will examine this choice of channel flux distribution, discuss its implications and drawbacks, and discuss an alternative: the uniform flux

$$\phi(\mathbf{r}) = \begin{cases} \frac{\phi_0}{V_{ch}}, & r < R_{ch} \\ 0, & r > R_{ch} \end{cases}$$

with $V_{ch} = \frac{4}{3}\pi R_{ch}^3$ the volume of the channel and ϕ_0 the same value as for the point source.

2.4.2 Localized flux

The most common and, perhaps, simplest distribution for modeling the calcium flux due to an open channel is a point source:

$$\phi(\mathbf{r}) = \phi_0 \cdot \delta^3(\mathbf{r})$$

The primary advantage to this distribution is that the reaction-diffusion equation

$$\frac{\partial c}{\partial t} = D\nabla^2 c - k^+ bc + k^-(B - b) + \phi_0 \cdot \delta^3(\mathbf{r})$$

for the calcium concentration due to a single open channel with this flux distribution, located in the center of a large domain, has the analytic steady-state solution

$$c(r) = c_0 + \frac{\phi_0}{2\pi D}\frac{e^{-\sqrt{\frac{k^+ b}{D}}r}}{r}$$

where $c_0 = \frac{k^-}{k^+}\frac{B-b}{b} = K\frac{B-b}{b}$. A derivation of this solution may be found in Appendix B.

This solution, while very easy to implement outside a channel, has the drawback of becoming singular at $r = 0$ and therefore has a wide (indeed, infinite) range of values within the domain of the channel. However, we know that the dynamics of the channel depend strongly on the local calcium concentration (Fig. 1.5). Consequently, it is important to find a method to select the value of the concentration at the channel.

Skupin et al. (2010) do not use the analytic solution, but nevertheless assume localized sources for the purpose of exploiting their ease of use with a Green's function approach to modeling the diffusion of calcium and buffers through the cytoplasm. As a result, the singularity at the channel is something they were forced to address

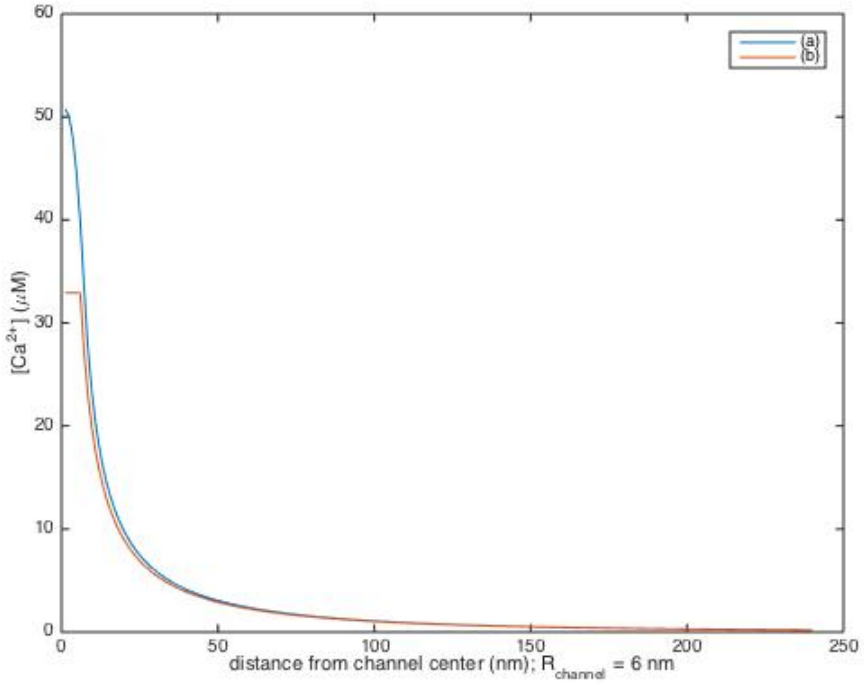

Figure 2.8: Steady state-concentration due to influx of a single open channel with the flux (a) spread uniformly over the channel volume, (b) localized at the channel center. For the localized source, the concentration profile is truncated at the channel boundary.

in the implementation of their model, and they chose to assign the value of the concentration at an open channel equal to the value at a distance some fraction of the channel radius away from the center of the channel.

This approach is rather difficult to use, as one must justify the distance chosen: a typical concentration at the boundary of an open channel might be 30 μM (Fig. 2.8). Comparing this value to Figure 1.5, we see that even with this range of possible values, there is wide variation in the possible dynamics, and therefore a value must be selected without arbitrariness, and this is impossible to accomplish solely considering localized sources.

Thus, although a point source seems at first glance to be mathematically simple to use, it proves to be a difficult choice when accuracy is taken into consideration.

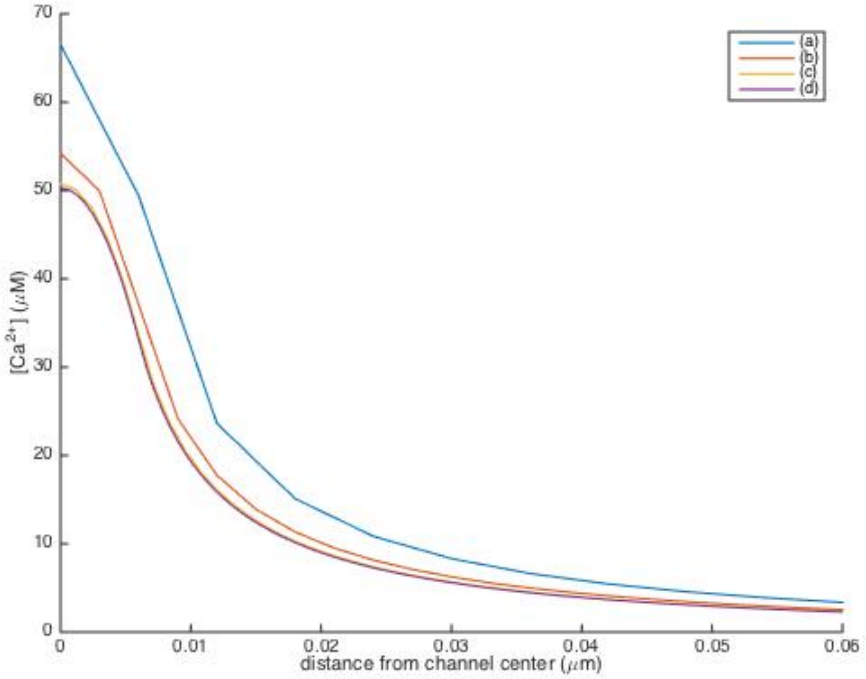

Figure 2.9: Steady state profile due to an open channel with uniform flux using a spatial granularity of (a) R_{ch}, (b) $\frac{R_{ch}}{2}$, (c) $\frac{R_{ch}}{5}$, (d) $\frac{R_{ch}}{10}$.

2.4.3 Uniform flux

Due to the difficulties in implementing a point source for the channel flux, we therefore examined spreading out flux uniformly over the domain of the channel. For simplicity (in order to maintain spherical symmetry), we chose to let the flux be nonzero over the region $r < R_c$ where R_c is the channel radius. That is, we replaced the flux density term

$$\phi_0 \, \delta^3(\mathbf{r})$$

with one of the form

$$\phi(\mathbf{r}) = \begin{cases} A\phi_0, & r < R_{ch} \\ 0, & r > R_{ch} \end{cases}$$

To find the value of A, we recognize that the total flux over the volume should be the same in both cases, and so we easily find that $A = (V_{ch})^{-1}$ where $V_{ch} = \frac{4}{3}\pi R_{ch}^3$.

This is very straightforward to implement numerically, and, with a sufficiently fine spatial granularity, reproduces the analytic profile outside of the channel with a great deal of accuracy (Fig. 2.8). Inside the channel, the profile remains finite and smooth with a peak at $r = 0$ that we can then select as the concentration at the channel.

We briefly note that our choice of flux distribution may be viewed as one of a family of functions approximating the Dirac delta distribution - that is, it is one member of a *Dirac sequence* - with compact support on the domain of the channel. One could use the framework of Dirac sequences to systematically study different flux distributions by, for example, constructing a generating function with compact support on the channel domain based on biological considerations (for instance, nonincreasing from channel center to channel boundary), and varying the sequence parameter to match experimental results. See, for instance, (Dang and Ehrhardt, 2012) for a short treatise on Dirac sequences and their generators.

It may be tempting to simplify the uniform flux approach back in the direction of a point source by choosing the spatial granularity coarsely enough such that the channel volume comprises the entire central volume element, so that all of the flux occurs in this one volume element. Figure 2.9 shows that this approach (i.e., setting $dr = R_{ch}$) introduces up to 30% error. In contrast, the spatial profile has a high degree of accuracy even with a mesh not much finer than this ($dr = \frac{R_{ch}}{5}$). This allows a spatial profile to be computed quite quickly and, when used in combination with the instantaneous equilibration approximation examined in Section 2.2, yields an effective modeling approach for the overall problem.

2.5 Puffs as the fundamental event

2.5.1 Motivation

Channels in the same cluster are packed closely to one another and so feel the effects of each other quite strongly. Indeed, because of the bursting nature of blips and the short time in which an open channel's concentration profile decays, it is difficult to see how a puff event could occur were the channels in a cluster not strongly coupled. In fact, experimental evidence (Watras et al., 1991) shows that puffs are the predominant event type in clusters, providing further evidence for this coupling.

Although channels in a cluster are strongly coupled, the coupling between clusters, is comparatively weak: the typical distance between clusters is around 1-3 μm (Dupont et al., 2011, Swillens et al., 1999), which suggests that the transition from puff level to spike level exhibits a much smaller degree of cooperativity than the transition from blip level to puff level. Because of the strongly concerted action of channels with a cluster, and the stark contrast of this behavior to that at the cellular level, it seems reasonable to treat an entire cluster as one object.

Furthermore, a typical cell has a few tens of clusters, a typical cluster has around 10-30 channels, and each channel has four subunits that at any timestep has three possible transitions it can take (or more, depending on the exact model, e.g., (Swillens et al., 1999), which includes additional binding sites and cooperativity). This results in an overwhelmingly large state space for the stochastic process. Additionally, because a channel's state depends on the combined states of its subunits, the majority of state transitions don't cause a channel to open or close, and so do not actually effect a change in the dynamics of the cell.

Between the large state space and the strong coupling between nearby channels, it makes sense to cultivate statistics for puffs from a single cluster, and use those

statistics to drive cluster dynamics when modeling a full cell. That is, we attempt to construct a full cellular model where each cluster is an isolated, holistic stochastic object, and individual channels are not explicitly included.

To do this, we assign to each cluster states corresponding to the number of open channels, ranging from 0 to the number of channels per cluster (typically 15-25). In numerical computations, the state number typically does not exceed 7 because the probability of additional channels opening simultaneously becomes exceedingly rare; the average puff consists of only five channels acting in concert. This reduces the number of states per cluster from around $25 \cdot 4 \cdot 8 = 800$ (depending on the model) down to only 8, resulting in a model that is significantly faster.

2.5.2 Computation of the cluster transition rates

To compute the cluster transition statistics, we model a cluster of individual channels for a sufficiently long simulation time and record the number of open channels at each timestep. From this data, we construct transition rates for the cluster (i.e., rate constants to go from j open channels to k open channels) as follows:

Suppose a stochastic process is in a given state, j, out of n total states, and the rate constant to transition from the j^{th} to the k^{th} state is α_{jk}, then the expected time to leave the current state is

$$\tau_j \equiv \left(\sum_{k=1}^{n} \alpha_{jk} \right)^{-1}$$

and the probability of transitioning to the k^{th} state instead of another is

$$P_{jk} = \frac{\alpha_{jk}}{\sum_{k=1}^{n} \alpha_{jk}} = \alpha_{jk} \tau_j$$

From the data we collect, it is straightforward to extract the time the cluster spends with a certain number of channels open and whether it then opens a new channel or closes one that is firing. It is then simple to compute the average time the cluster spends with j channels firing before opening or closing one - which is precisely τ_j - and the relative frequency with which it opens a new channel instead of closing a firing one: if $n_{j,k}$ is the number of times the cluster goes from j open channels to k open channels (where k is necessarily either $j-1$ or $j+1$), then the frequency for opening a new channel is

$$f_{j,j+1} \equiv \frac{n_{j,j+1}}{n_{j,j-1} + n_{j,j+1}}$$

and similarly, the frequency for closing an active channel is

$$f_{j,j-1} \equiv \frac{n_{j,j-1}}{n_{j,j-1} + n_{j,j+1}}$$

It is reasonable to assume that this process is ergodic; every state is clearly recurrent, and although under the Gillespie algorithm, the states are periodic (with period 2) by construction, were we to choose a uniform timestep for the Markov chain, there would be a nonzero probability of remaining in the same state (either having not changed, or having gone to another state and back in the same timestep, depending on the size of the timestep), and so the states would be aperiodic. Under this assumption, we have $f_{j,j\pm1} \approx P_{j,j\pm1}$ with equality holding in the limit as simulation runtime goes to infinity. We can therefore derive cluster transition rates by

$$\alpha_{j,j\pm1} = \frac{f_{j,j\pm1}}{\tau_j}$$

provided we run the simulation for a sufficient amount of time. Now that we have computed the cluster transition rates, we can apply the same overall approach we used for modeling the stochastics of channels to the reduced problem where each source is assumed to be an entire cluster.

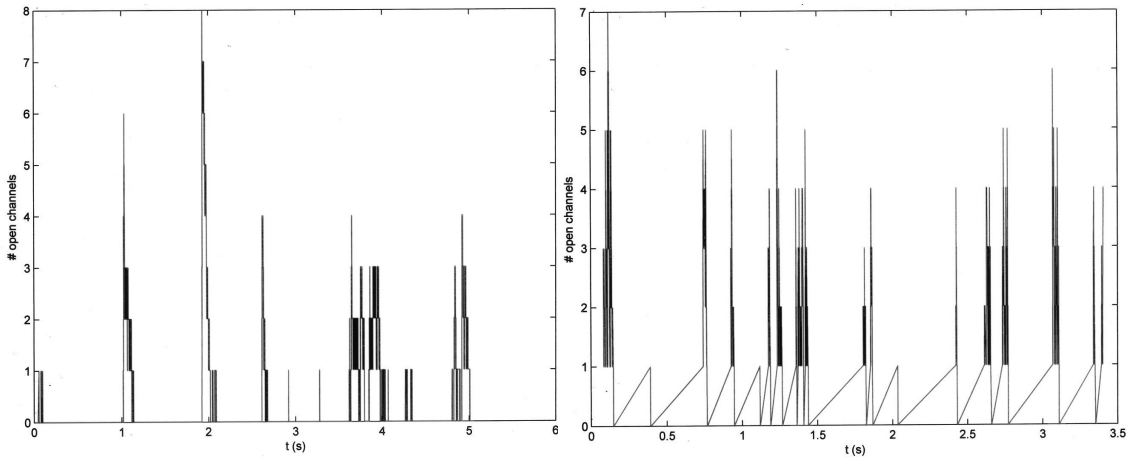

(a) (b)

Figure 2.10: A comparison of the resulting dynamics modeling a cluster as (a) consisting of 25 channels and using the traditional De Young-Keizer model, (b) a single stochastic object with transition rates as computed in Section 2.5.2. Note: the steep diagonal lines in part (b) result from automatic linear interpolation between two distant data points; the concentration is actually c_0 on these intervals.

2.5.3 Results

The most straightforward way to verify this approach is to run a simulation with this approach and compare the results to those of a simulation incorporating stochastics of individual channels. Such a comparison may be found in Figure 2.10. Both of these models assume a single cluster in the center of a spherical cell-sized domain with Dirichlet boundary conditions. The biological parameters used are from (Swillens et al., 1999). The states were evolved using the Gillespie algorithm and the calcium concentration was evolved assuming instantaneous equilibrium, and so the total number of open channels was tracked as a function of time (since the spatial extent of the equilibrium profile is much smaller than the radius of the cell, and therefore the average calcium concentration in the cell is precisely proportional to the number of open channels).

It is apparent that the results of these two simulations are not dissimilar; the most significant difference between the two is the frequency of puff events, which

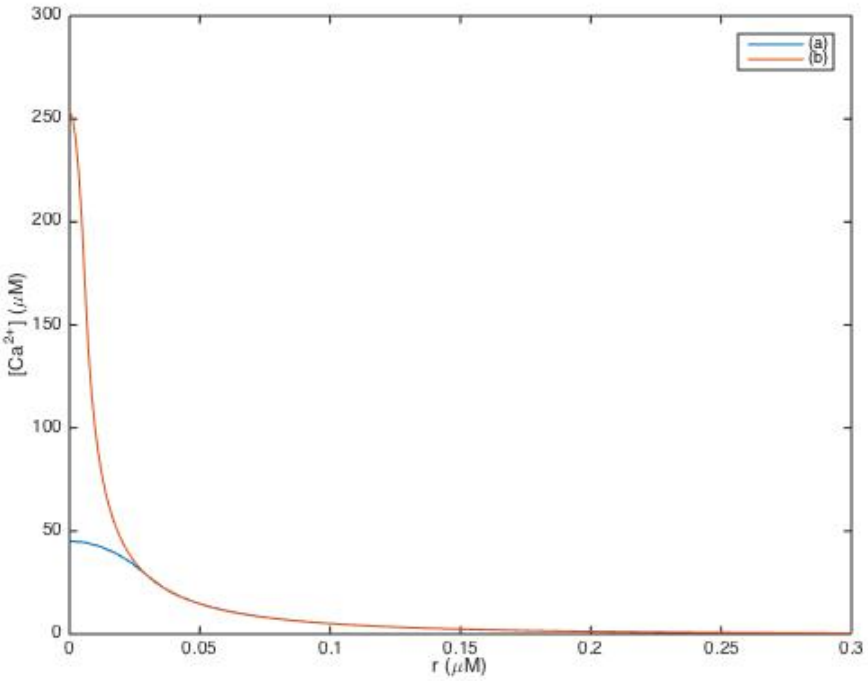

Figure 2.11: Steady-state spatial profile due to a 5-channel-strength source (typical puff size) with the flux spread uniformly over (a) the volume of the cluster and (b) the volume of a single channel. The radius of a cluster is 30 nm.

are roughly twice as frequent in the simplified cluster model (the reason for this discrepancy is still unclear). However, these two schemes show excellent agreement in terms of amplitude and duration of puffs, as well as ratio of puffs to blips.

The primary computational expense of the general model, however, is not the stochastic part of the simulation, but the diffusion, if we do not use the assumption of instantaneous equilibration. By averaging the stochastic behavior of a cluster over its entire domain, we treat the cluster as a single source, the strength of which depends on the stochastic state of the cluster. The radius of a cluster is an order of magnitude larger than the radius of a single channel, and we can exploit that by averaging the cluster source over its volume - instead of over a volume the size of a channel - and then choose a much coarser mesh for modeling the diffusion. Figure 2.11 shows that, outside the cluster radius, the two spatial profiles agree closely.

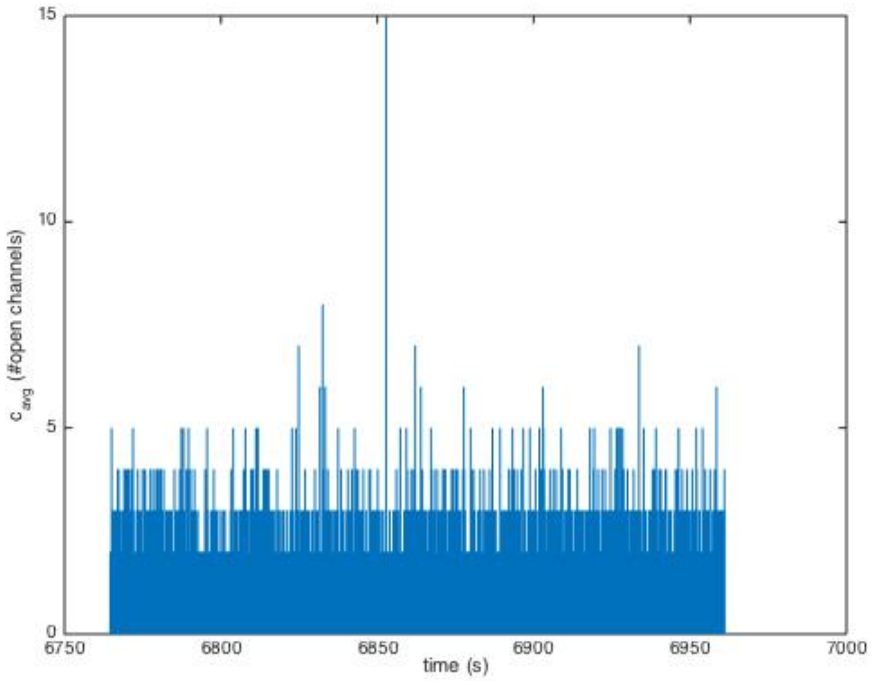

Figure 2.12: A spike.

Finally, we employed this approach to modeling a cluster in a simulation of a cell with 50 clusters in it. Notably, this simulation - modeling an entire cell - was run in less than an hour on a laptop. An excerpt of the resulting cellular concentration profile as a function of time may be seen in Figure 2.12. Because the average puff event peaks at approximately five channels (which is consistent with Figure 2.12), the one event with 15 open channels is likely due to the simultaneous activation of three separate clusters. In other words, this event is likely a spike.

Although this simulation saw only one spike in over two hours of simulation time (compared the expected timescale of minutes), it provides a proof of concept for this approach and demonstrates that CICR spikes may be simulated with a computationally inexpensive approach. Future work may adapt this sufficiently to produce qualitatively or even quantitatively correct results.

Chapter

THREE

Channel Reaction Rates

3.1 Overview

In Chapter 2 we examined and discussed several approximations that could be used to make a model of CICR simpler and computationally less expensive. We discussed the implications of these approximations and justified their use by analyzing their accuracy in modeling CICR compared to more traditional, more exact choices. Conversely, in this chapter, we aim to make CICR models more precise by examining closely one key aspect of the model: the channel reaction rates.

One of the most critical choices to make in modeling calcium channels is the set of binding and dissociation rates of molecules to the receptor sites at a channel. These rates have a dramatic impact on the channel dynamics since the ratios of these quantities determine the relative amount of time spent in each state as well as, perhaps most importantly, the driving factors for the opening or closing of a channel.

Furthermore, there appears to be very little agreement in the literature about the values of these transition rates (Table 3.2), which reflects little collective understanding of the interactions of individual molecules and ions with the channel receptors. For most of the transition rates, the literature does not agree even on the order of magnitude of these values. We therefore attempted, following the work of Swillens et al. (1999), to derive values for these rates based on experimental evidence, adapting their method for a tetrameric channel structure.

In addition to providing a starting point for constructing models of CICR, this method for selecting the rate constants may be used to probe more precisely the inner workings of the calcium channel receptor reaction dynamics.

3.2 Illustration

In this section, we will examine the choices made for the values of binding and dissociation rates in one particular model, as an illustration of the importance of selecting these values carefully.

Skupin et al. (2010) used the following transition rates (table recreated from supporting text for (Skupin et al., 2010)):

a_1	20	$\mu M^{-1}s^{-1}$	IP_3 binding with no inhibiting Ca^{2+} bound
b_1	20	s^{-1}	IP_3 dissociation with no inhibiting Ca^{2+} bound
a_2	.001	$\mu M^{-1}s^{-1}$	Ca^{2+} binding to inhibiting site with IP_3 bound
b_2	.03	s^{-1}	Ca^{2+} dissociation from inh. site with IP_3 bound
a_3	2.6	$\mu M^{-1}s^{-1}$	IP_3 binding with inhibiting Ca^{2+} bound
b_3	20	s^{-1}	IP_3 dissociation with inhibiting Ca^{2+} bound
a_4	.025	$\mu M^{-1}s^{-1}$	Ca^{2+} binding to inhibiting site with no IP_3 bound
b_4	.1	s^{-1}	Ca^{2+} dissociation from inh. site with no IP_3 bound
a_5	10	$\mu M^{-1}s^{-1}$	Ca^{2+} binding to activating site
b_5	1.225	s^{-1}	Ca^{2+} dissociation from activating site

Table 3.1: Channel transition rates from Skupin et al. (2010). Refer to Figure 3.1 for a schematic illustrating the behavior of channel transitions.

This model used an IP_3 concentration of .1 μM and a base calcium concentration of .05 μM. There are several important implications to the stochastic channel dynamics. The most notable, perhaps, is that with an IP_3 concentration of $[IP_3] = .1$ μM, the binding rate for an *uninhibited* subunit is only 2 s^{-1} compared to a 20 s^{-1} dissociation rate. Consequently, the subunit has only a 9% chance of having IP_3 bound at any given moment, and this is independent of any of the channel or cell dynamics. Because a tetrameric channel requires the concerted activation of three or more subunits in order to open, the probability of the channel having sufficient IP_3 bound to be capable of opening is then only 0.28%, or about 1 in 350. There are generally around 10-30 channels in each cluster, which means that having more than one channel in a cluster simultaneously open is rare with this model.

Additionally, even when all the channels are closed and the cell is at equilibrium, the binding rate of calcium to the activating site is .5 s^{-1} compared to a dissociation rate of 1.2 s^{-1}, so when the cell is at equilibrium, there's a roughly 40% chance of a channel subunit having activating calcium bound - four times more likely than the same probability for IP_3. When the channel opens, the probability of having activating calcium bound rises to 90+%, but the IP_3 distribution remains the same, which means that a channel opening doesn't dramatically influence the firing probability of itself or other nearby channels; this model has extremely weak interchannel coupling.

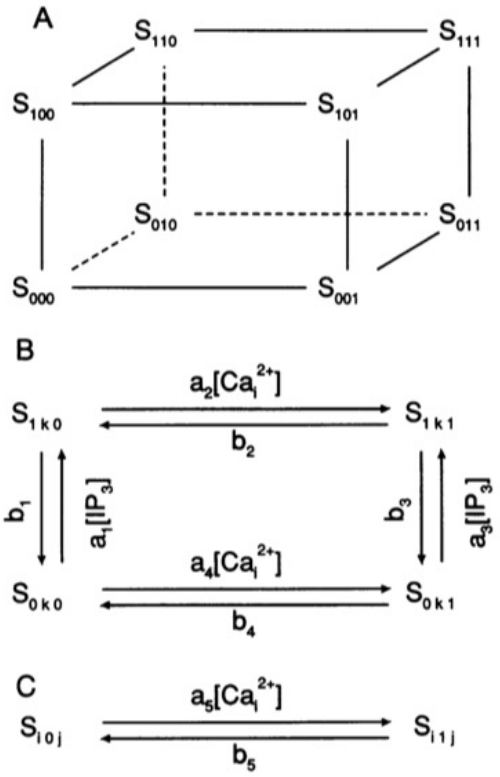

Figure 3.1: The original De Young-Keizer model. The quantities a_j are binding rates and the b_j are dissociation rates. Figure recreated from (De Young and Keizer, 1992). (Repeated from Chapter 1.)

Because the influence of a single channel decays rapidly upon closure of the channel, if the channels themselves have weak coupling, then puffs (and therefore spikes) can only occur by coincidental simultaneous opening of multiple channels, which runs counter to the common intuition that a channel opening should provoke other channels to open.

	(a)	(b)	(c)	(d)		(e)
a_1	20	400	80	20	k_i^+	35.8
b_1	20	52	.64	52	k_i^-	5
a_2	.001	.2	.04	.001	k_d^+	.088
b_2	.03	.2098	.48	$3.077{\cdot}10^{-4}$	k_d^-	1.67
a_3	2.6	400	80	20	k_i^+	35.8
b_3	20	377	40	52	k_i^-	5
a_4	.025	.2	.4	.025	k_d^+	.088
b_4	.1	.0289	.0768	.0025	k_d^-	1.67
a_5	10	20	15	10	k_a^+	166
b_5	1.225	1.647	12	122.5	k_a^-	65.9

Table 3.2: Comparison of channel rate constants from various models: (a) Skupin et al. (2010), (b) De Young and Keizer (1992), (c) Rüdiger et al. (2007), (d) Thurley and Falcke (2011), (e) those computed in this chapter. As before (Tables 1.1, 3.1), the a_i are binding rates and have units $\mu M^{-1}s^{-1}$ and the b_i are dissociation rates with units s^{-1}. Note: many articles list values of a_i and d_i where $d_i \equiv \frac{b_i}{a_i}$. For these articles, we have instead computed and listed the values of b_i for easier comparison. We have included the corresponding nomenclature used in this chapter for convenience.

3.3 Construction

Introduction

In this section, we will look at data from experiments on calcium channels, and use this data to derive values for the channel transition constants. For this construction, we assume the usual eight-state DeYoung-Keizer model, and we assume precisely zero cooperativity. That is, one receptor being bound neither directly helps nor directly inhibits the binding of other receptors. In the context of the above table, this would mean that $a_1 = a_3$, $b_1 = b_3$, $a_2 = a_4$, and $b_2 = b_4$. Therefore, we seek values for six transition rates in total, which describe mutually independent stochastic events. Following the nomenclature of Swillens et al. (1999), we label these rates $k_i^\pm$ for binding and dissociation of IP_3, $k_a^\pm$ for binding and dissociation of Ca^{2+} at the activating site, and $k_d^\pm$ for binding and dissociation of Ca^{2+} at the

deactivating (inhibiting) site. Table 3.2(e) lists the values for these rates that we will construct in this section, with the nomenclature used in this chapter included for convenience.

Probability of opening

We start with the assumption that $k_i^- = 5\ \mathrm{s}^{-1}$ (Hannaert-Merah et al., 1995), which we note is well within the range of values for b_1 in Table 3.2. We can then compute k_i^+ from a consideration of puff amplitude: if we take the number of channels in a cluster to be 25, we take the size of a puff to be 5 times that of a blip, and we assume that most cluster events are puffs (that is, we assume strong coupling between channels in a cluster), then it follows that at any given moment, we expect on average one fifth of the channels to have IP_3 bound to three or more subunits (so that the channel will open if flooded with calcium), and so each channel should have a probability of $\frac{1}{5}$ of being in such a state.

The models Swillens uses does not have a subunit structure (the channel is monomeric), so the computation of k_i^+ is straightforward: the aforementioned probability is precisely $\frac{k_i^+[\mathrm{IP_3}]}{k_i^+[\mathrm{IP_3}]+k_i^-} = \left(1+\frac{K_i}{[\mathrm{IP_3}]}\right)^{-1}$, where $K_i \equiv \frac{k_i^-}{k_i^+}$ is the dissociation constant for this reaction. We can then set this quantity equal to $\frac{1}{5}$ and easily solve for k_i^+. With a tetrameric structure, the computation is only slightly more complicated. We define the following probabilities: p_a is the probability that the channel has sufficiently many IP_3-bound receptors to be open (contingent upon calcium binding), p_n is the probability that precisely n subunits are IP_3-bound, and $p = \left(1+\frac{K_i}{[\mathrm{IP_3}]}\right)^{-1}$ is the probability for one specific subunit being bound. Then we have:

$$p_n = \binom{4}{n} p^n (1-p)^{4-n}$$

and so

$$\begin{aligned} p_a &= p_3 + p_4 \\ &= 4p^3(1-p) + p^4 \\ &= 4p^3 - 3p^4 \end{aligned}$$

Taking $p_a = \frac{1}{5}$, we find $p = .41755$ (of the remaining roots, two are complex and the other is greater than 1). Setting

$$\left(1 + \frac{K_i}{[\mathrm{IP}_3]}\right)^{-1} = .41755$$

we then determine a value of $k_i^+ = 35.8\,\mu\mathrm{M}^{-1}\mathrm{s}^{-1}$ for a tetrameric channel with a cellular IP_3 concentration of .1 μM.

Mean open time

We can determine two more rate constants, namely k_a^- and k_d^+, from consideration of the mean open time of a channel. There are three ways an active subunit can deactivate, causing the channel to close: dissociation of IP_3, dissociation of Ca^{2+} from the activating receptor, and binding of Ca^{2+} to the inhibiting receptor. The expected rate for a subunit deactivation is the sum of the rates of these three processes, i.e., $k_i^- + k_a^- + k_d^+[\mathrm{Ca}^{2+}]$, and so the rate for channel closing is then $3(k_i^- + k_a^- + k_d^+[\mathrm{Ca}^{2+}])$, assuming that precisely three subunits are active and that a fourth subunit does not activate before a currently active subunit deactivates.[1] Consequently, the mean open

[1] Correcting for the possibility of four subunits being active would require a much more sophisticated approach that would necessarily involve all of the rate constants, due to the possibility of repeatedly bouncing between three and four active subunits. However, the probability of a channel having four simultaneously active subunits is bounded above by 3% (the probability of having IP_3 bound to all four subunits), and so the correction to the rate constants should be small.

time for a channel can then be expressed as

$$T_{\text{open}} = \frac{1}{3}\left(k_i^- + k_a^- + k_d^+[\text{Ca}^{2+}]\right)^{-1}$$

We already have a value for k_i^- ($5\ \text{s}^{-1}$), so two data points suffice to compute the other two rates. Swillens cites a patch clamp experiment (Bezprozvanny and Ehrlich, 1994) measuring mean channel open time as a function of cytosolic calcium concentration. With a concentration of $[\text{Ca}^2+] = .2\ \mu\text{M}$, the mean open time was found to be 4.7 ms, and with a concentration of 500 μM, the mean open time was 2.9 ms. Using these values, we find $k_a^- = 65.9\ \text{s}^{-1}$ and $k_d^+ = .088\ \mu\text{M}^{-1}\text{s}^{-1}$.

Opening latency

To determine k_a^+, Swillens examined an experiment (Callamaras et al., 1998) wherein a cluster of calcium channels was suddenly flooded with a controlled concentration of IP_3 and the time needed for any channel to open was then measured. As the amount of IP_3 introduced increased, the latency steadily decreased to a limiting value of about 80 ms. This implies that IP_3 reaches saturation at a certain threshold, at which all channels have IP_3 maximally bound, and channel opening is then gated by calcium binding to the activating receptors. For monomeric channels, this once again leads to a very straightforward computation for k_a^+. Assume a cluster with 25 channels and a base calcium level of .04 μM. Then, if IP_3 is already bound, the expected time for the channel to open is the same as the expected time for activating calcium to bind:

$$t_{ch} = \frac{1}{k_a^+[\text{Ca}^{2+}]}$$

and the expected time for any channel in the cluster to fire is $\frac{t_{ch}}{N}$ where N is the number of channels. So in this case, $k_a^+ = (25 \cdot .08\ \mathrm{s} \cdot .04\ \mu\mathrm{M})^{-1} = 12.5\ \mu\mathrm{M}^{-1}\mathrm{s}^{-1}$.

Adapting this for a tetrameric channel is dramatically more complicated both because the channel can take a lot of different paths through the state space to get to an open state, and because there is more than one state each channel can start in, as opposed to simply the "off" state in the above approach. To approach this problem, we define the channel as having five states corresponding to the number of active subunits (0 – 4), and we seek to compute the time of first arrival to the state 3 from an arbitrary starting state.[2]

For each state n, we define the following characteristic times:

$$\begin{aligned} \tau_n &= \text{time to transition away from state } n \text{ to any other state} \\ \tau_n^0 &= \text{time to return to state } n \text{ after transitioning to state } n-1 \\ \tau_n^+ &= \text{time to first arrival at state } n+1 \text{ starting from state } n \end{aligned}$$

Additionally, we define P_n to be the probability of the channel starting in state n, which depends only on the initial calcium concentration and the transition rates.

With these definitions, the expected time to first channel opening is then

$$\tau_{\text{open}} = P_0(\tau_0^+ + \tau_1^+ + \tau_2^+) + P_1(\tau_1^+ + \tau_2^+) + P_2\tau_2^+$$

First, τ_n is simply (sum of rates of transitions away from n)$^{-1}$, i.e.,

$$\tau_n = \frac{1}{n \cdot k_a^- + (4-n) \cdot k_a^+ [\mathrm{Ca}^{2+}]}$$

[2] We do not actually need to consider the state 4 because the "off" states - 0, 1, and 2 - cannot transition directly to 4 without going to 3 first. If the channel starts in state 3 or state 4, it will fire immediately upon binding IP_3, and there will be no contribution to the average latency.

For brevity, for the rest of this section, we will take k^+ to mean $k_a^+[\mathrm{Ca}^{2+}]$ and k^- to mean k_a^-, since the calcium concentration is constant for this problem and since we are only concerned with the dynamics of the activating calcium receptors. Then

$$\tau_n = \frac{1}{nk^- + (4-n)k^+}$$

For the state 0, the only transition possible is to the state 1, so we have $\tau_0^0 = 0$ and $\tau_0^+ = \tau_0$. For the rest of the states, the time to return to the state n after transitioning backwards to $n-1$ is the time to transition away from n plus the time of first arrival from $n-1$ to n. That is,

$$\tau_n^0 = \tau_n + \tau_{n-1}^+$$

To compute τ_n^+, we need to consider that the channel may go back to $n-1$ an arbitrarily large number of times before proceeding to $n+1$. The probability of transitioning from n to $n-1$ is

$$p_n = \frac{nk^-}{nk^- + (4-n)k^+} = nk^-\tau_n$$

and the probability of transitioning from n to $n+1$ is

$$1 - p_n = (4-n)k^+\tau_n$$

Suppose the channel goes back to $n-1$ a total of j times before going to $n+1$. The probability of this occurrence is

$$(1-p_n)(p_n)^j$$

and the expected time for this process to elapse is

$$\tau_n + j\tau_n^0$$

Therefore, the expected first arrival time from n to $n+1$ is given by

$$\begin{aligned}
\tau_n^+ &= \sum_{j=0}^{\infty}(1-p_n)(p_n)^j(\tau_n + j\tau_n^0) \\
&= (1-p_n)\left(\tau_n\sum_{j=0}^{\infty}(p_n)^j + \tau_n^0\sum_{j=0}^{\infty}j(p_n)^j\right) \\
&= (1-p_n)\left(\frac{\tau_n}{1-p_n} + \frac{p_n\tau_n^0}{(1-p_n)^2}\right) \\
&= \tau_n + \frac{p_n}{1-p_n}\tau_n^0 \\
&= \frac{1}{1-p_n}\tau_n + \frac{p_n}{1-p_n}\tau_{n-1}^+ \\
&= \frac{1}{(4-n)k^+} + \frac{nk^-}{(4-n)k^+}\tau_{n-1}^+
\end{aligned}$$

Thus, we have

$$\begin{aligned}
\tau_0^+ &= \frac{1}{4k^+} \\
\tau_1^+ &= \frac{1}{3k^+} + \frac{k^-}{3k^+}\left(\frac{1}{4k^+}\right) \\
\tau_2^+ &= \frac{1}{2k^+} + \frac{k^-}{k^+}\left(\frac{1}{3k^+} + \frac{k^-}{3k^+}\left(\frac{1}{4k^+}\right)\right)
\end{aligned}$$

Analogously to before, when examining IP_3 transitions, we have that P_n (the probability at equilibrium of n subunits having calcium bound to the activating site) is given by

$$P_n = \binom{4}{n}\left(\frac{k^+}{k^+ + k^-}\right)^n\left(\frac{k^-}{k^+ + k^-}\right)^{4-n}$$

Thus, we have reduced our expression for τ_{open} to one involving only k^- and k^+. Furthermore, we have already computed the value of k^-. Recall:

$$k^- \equiv k_a^- = 65.9 \text{ s}^{-1}$$

The latency time for the experiment was reported as 80 ms, so if the cluster size is 25 channels, then the expected latency of a single channel should be $\tau = 25 \cdot 80 \text{ ms} = 2 \text{ s}$. Using these values for τ and k^-, we can solve for k^+ readily, for instance by using a software algebra system. The resulting value for $k^+ \equiv k_a^+[\text{Ca}^{2+}]$ was found to be 6.64 s^{-1}. Since the experiment in (Callamaras et al., 1998) took place with a base calcium concentration of .04 μM, it then follows that $k_a^+ = 166\,\mu\text{M}^{-1}\text{s}^{-1}$.

Recovery time

It remains to find a value for k_d^-. The primary effect of this parameter is clear; binding of calcium to the inhibiting sites of channels in an active cluster provides a mechanism to turn off that cluster, so the rate of dissociation of calcium from these sites determines a "recovery time" - the amount of time after the cluster shuts down before it can become active again.

Swillens argues that when a cluster ceases activity, most or all of the channels in the cluster are desensitized - that is, they have calcium bound to the inhibiting receptors. This has the important implication that, once a cluster has become desensitized, a channel should recover much more quickly than the expected activation time for a channel. If this were not the case, then individual channels could fire upon recovery while the rest of the cluster was still desensitized, and therefore there would be a greater proportion of blips than experimentally observed.

If we assume that most subunits are desensitized when a puff ceases activity,

then a channel will resensitize when three subunits resensitize. Thus, the criterion of fast channel resensitization is that the time for three subunits to resensitize is much faster than the single-channel latency. Recall that the expected latency for a single channel is 2 s. Therefore, we have:

$$3k_d^- \gg \frac{1}{2\text{ s}} = .5\text{ s}^{-1}$$

so $k_d^- \gg .167\text{ s}^{-1}$. This gives us one bound on k_d^-. To find another, we simply note that a cluster ought to be able to become fully desensitized on a reasonable timescale. This means that at calcium concentrations typical for a puff, after sufficient time has elapsed for the states to be well mixed, we should find a high proportion of subunits in an inhibited state. In other words, at these concentration levels, the probability of having calcium bound to the inhibiting site of any subunit should be relatively high.

Assuming a cluster consists of a 5×5 array of directly adjacent channels, the average pairwise distance between channels is roughly $5R_{ch} = .03$ μm. The value of the steady-state distribution at this distance from an open channel is 5.3 μM. If we take this as the average concentration on a channel due to an open channel anywhere in the cluster, then the average concentration due to a puff event (equivalent to five open channels) would be 26.5 μM, and the binding rate to an inhibiting site would then be $k_d^+[\text{Ca}^{2+}] = (.088\ \mu\text{M}^{-1}\text{s}^{-1})(26.5\ \mu\text{M}) = 2.33\text{ s}^{-1}$.

Taking $k_d^- = 1.67\text{ s}^{-1}$ (i.e., an order of magnitude higher than the previously derived constraint), and assuming a well-mixed state during a puff event, we then find the probability of an individual subunit not having inhibiting calcium bound to be

$$p \equiv \left(1 + \frac{[\text{Ca}^{2+}]}{K_d}\right)^{-1} = .426$$

and the probability of a channel being desensitized is then

$$\begin{aligned}\text{Prob(2 or more subunits inhibited)} &= 1 - \text{Prob(0 or 1 subunits inhibited)} \\ &= 1 - (4p^3 - 3p^4) \\ &= .790\end{aligned}$$

so about $\frac{4}{5}$ of channels are desensitized after a sufficient amount of time has elapsed during a puff, which seems reasonable.

As a final check, the same probability during equilibrium when channels are closed (using a base calcium concentration of .05 μM) is only .0000413 - as expected, the probability of a channel being desensitized is vanishingly small during cell equilibrium. Therefore, we are justified in taking $k_d^- = 1.67\ \text{s}^{-1}$.

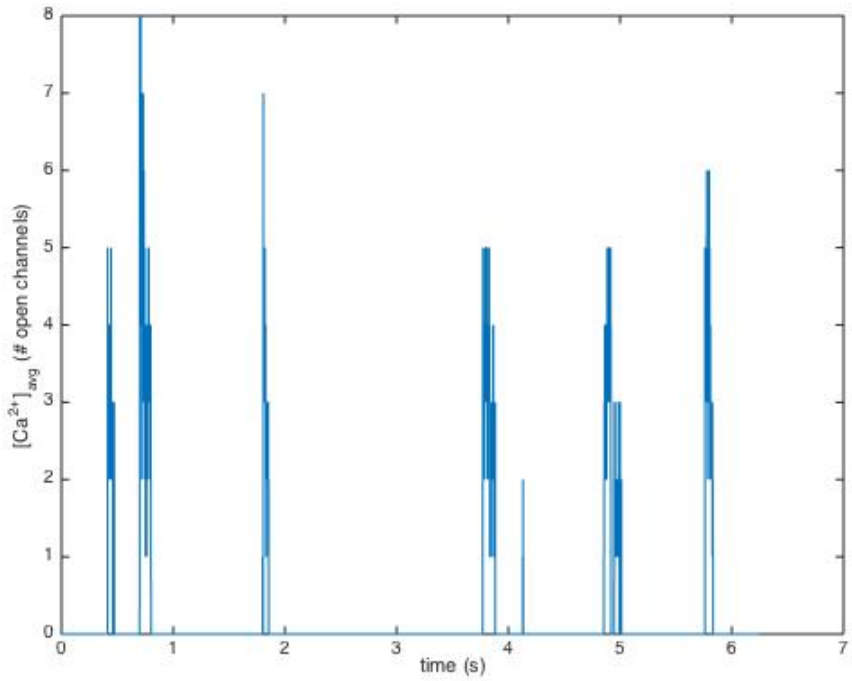

Figure 3.2: Dynamics of a single cluster with transition rates for tetrameric channels derived from experimental data.

3.4 Results

We have now succeeded in constructing a full set of stochastic channel transition rates (Table 3.2(e)) from consideration of experimental results concerning various significant expected times. To test the validity of these rates, we incorporated them into a model of a single cluster of channels.

The model used is the same as that for Figure 2.10a except for the choice of channel reaction rates: the biological parameters are taken from (Swillens et al., 1999), and we model a single cluster in the center of a cell-sized domain with Dirichlet boundaries. Instantaneous equilibration is assumed, and the stochastic process is governed by the binding and dissociation rates constructed in this chapter.

Figure 3.2 shows an excerpt of the evolution of the average cellular concentration

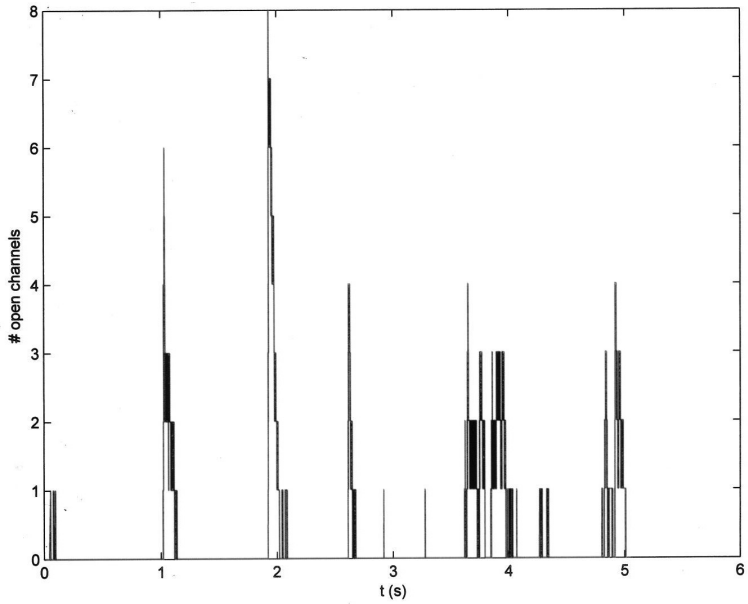

Figure 3.3: Dynamics of a single cluster with parameters from (Swillens et al., 1999). Repetition of Figure 2.10a.

due to the activity of this cluster. Comparison with Figure 3.3 shows that these rates produce results consistent with those of other models.

Chapter

FOUR

Conclusion

4.1 Summary

We have in this work examined several approximations, simplifications, and methods for modeling aspects of calcium-induced calcium release. To reiterate, our primary results were:

- The assumption that the calcium concentration immediately equilibrates to a steady-state spatial profile upon the opening or closing of a single channel is a useful and reasonable approximation.
- The assumption that the concentrations of any buffer species do not depend on location or time is a useful and reasonable approximation.
- It is possible to model CICR treating a cluster as a single, fundamental stochastic object and obtain qualitatively reasonable results.
- The assumption that the single-channel flux is concentrated at a point is not a reasonable approximation and is of questionable usefulness. Instead, taking the flux to be uniform over the channel volume offers an approach with less arbitrariness that is neither computationally expensive nor difficult to implement.
- It is possible to construct channel receptor binding and dissociation rates for a cluster of channels using data from experimental results. The use of such a construction yields a working numerical model for a cluster of calcium channels.

When combining these results together, we can construct a full-cell model that can be executed start-to-finish in a reasonable amount of time on a home computer.

4.2 Full model

4.2.1 Single channel

The first step, after selecting values for the various biological parameters, is to construct the steady-state profile due to a single open channel. To accomplish this, we use a simple second-order finite difference scheme for the reaction-diffusion equations for the calcium and buffer concentrations. Here, we use the assumption of constant buffers to reduce the system to a single equation. Furthermore, we assume that the cell boundaries are sufficiently far away that we can employ radial symmetry to reduce the number of computed dimensions to 1, and additionally, that we can use Dirichlet boundary conditions, $c(R_{\text{cell}}) = c_0$.

We take the spatial step to be $dr = \frac{R_c}{5}$, where R_c is the channel radius, and assume a uniform flux within the channel radius. This manifests in the finite difference scheme as an extra term on the right-hand side for $r \leq R_c$.

We evolve the concentration in time using a fourth-order Runge-Kutta scheme. We evolve for a sufficiently long time - around 3 ms - for the spatial profile to reach equilibrium. We then store the resulting equilibrium profile to be recalled later.

4.2.2 Single cluster

Once we have the single-channel equilibrium profile, the next step is to compute the statistics for a single cluster of channels. We take a cluster to be a square array of 25 channels, directly adjacent to one another. We keep track of the calcium concentration at the center of each of the 25 channels.

Each channel is tetrameric - that is, it is comprised of four identical subunits.

k_i^+	35.8	$\mu M^{-1}s^{-1}$	IP_3 binding
k_i^-	5	s^{-1}	IP_3 dissociation
k_a^+	166	$\mu M^{-1}s^{-1}$	Ca^{2+} binding to activating site
k_a^-	65.9	s^{-1}	Ca^{2+} dissociation from activating site
k_d^+	.088	$\mu M^{-1}s^{-1}$	Ca^{2+} binding to inhibiting site
k_d^-	1.67	s^{-1}	Ca^{2+} dissociation from inhibiting site

Table 4.1: Summary of channel transition rates derived in Chapter 3.

Following the work of De Young and Keizer (1992), we consider each subunit of a channel to be in one of eight possible states, corresponding to the presence or absence of IP_3, activating Ca^{2+}, and inhibiting Ca^{2+}. The binding and dissociation of these species from the receptor sites is governed by the transition rates given in Table 4.1, which are those we derived in Chapter 3.

We use Gillespie's algorithm to determine the length of each timestep and compute the binding and dissociation reactions of the receptors throughout the cluster. After each event, we determine whether a channel has just opened or closed: if a channel has three or four subunits with IP_3 bound and Ca^{2+} bound to the activating site but not to the inhibiting site, it is considered to be open.

When a channel is open, we update the concentration at each channel using the distance between each pair of channels and the steady-state spatial profile we computed for a single channel. If the distance is not an integer multiple of $\frac{R_c}{5}$, we linearly interpolate between the two closest data points for the steady-state profile. The concentration at a channel is the sum of the effects of all currently open channels plus the base concentration level, as described in Section 2.2.4.

We run this simulation for a sufficiently long time - several seconds - to get a large amount of data, and we then compute the relative frequencies and average lengths of time for having different numbers of channels simultaneously open as detailed in Section 2.5. We repeat this process for a range of values of c_0 since, as demonstrated in Figure 4.1, the channel dynamics can vary widely as a function of c_0. We choose

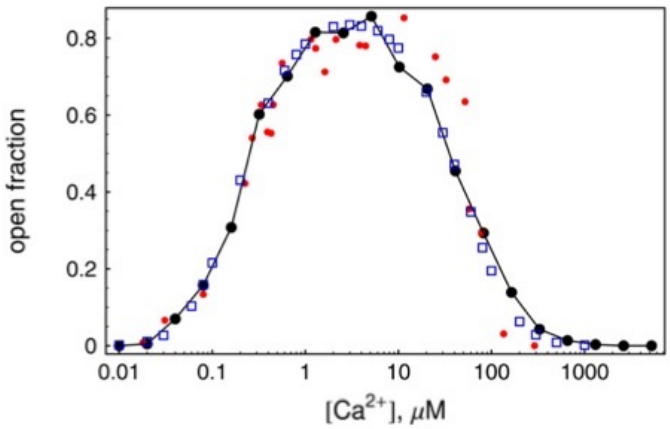

Figure 4.1: The fraction of time a single channel is open as a function of local calcium concentration. Repetition of Figure 1.5.

values of c_0 on a logarithmic scale in order to have finer granularity at concentrations close to the base concentration, since the effect of one cluster on another is usually rather subtle.

4.2.3 The cell

Once we have statistics for a cluster of channels, we can model a single cluster much more quickly (Fig. 2.10b) or model several clusters in a cell (Fig. 2.12). For the latter, we randomly distribute roughly 30-50 clusters uniformly in an area in the center of the cell, far enough from the cell boundaries that we can ignore their effect.

The statistics of a cluster change only due to the *base* local calcium concentration; the effect of an active cluster on itself is already accounted for in the cluster statistics, so we do not need to be careful about computing peak concentration at an active cluster as we did for an individual channel. Additionally, the equilibrium profile due to a source is, outside the flux region, independent of the flux distribution provided the total flux is the same (Fig. 4.2). For these reasons, we can treat the

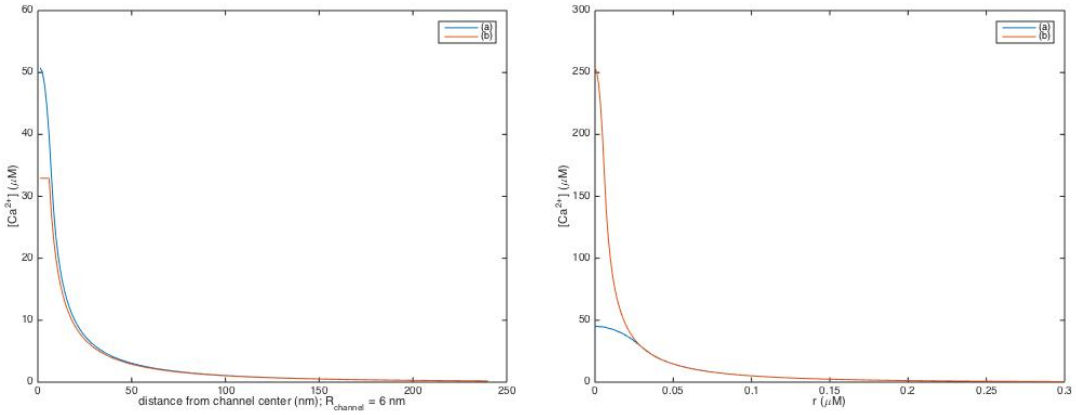

(a) (b)

Figure 4.2: A comparison of the spatial equilibrium profile for (a) a single channel with point source or uniform flux, (b) a cluster of channels with uniform flux over the volume of a channel vs. volume of a cluster. Repetition of Figures 2.8 and 2.11.

clusters as points, and so we keep track of the local calcium concentration at the center of each cluster.

We model the cell dynamics in the same way as we did the single-cluster dynamics: we use the cluster statistics together with the Gillespie algorithm to determine the length of each timestep and what happens at each timestep. The principle difference is that when a cluster undergoes an event, it does not have an effect on itself (again, because this is already accounted for in the cluster statistics). We compute the effect on other clusters using the distance between them, the single-channel steady-state profile, and the number of open channels. Since we are treating the cluster as a point, the profile for a cluster with n open channels is

$$c(r) = n(\tilde{c}(r) - c_0) + c_0$$

where $\tilde{c}(r)$ is the steady-state profile for a single channel.

More explicitly, at each timestep, we use the Gillespie algorithm to compute the length of the timestep and the next event, which will be equivalent to a channel

opening or closing, and be reflected in the state of the affected cluster. The calcium concentrations at every other cluster is then updated to reflect the new number of open channels in the affected cluster. Tracking the number of open channels at each timestep along with total elapsed time allows us to examine the time evolution of the average calcium concentration in the cell.

4.3 Further work

While we have succeeded in probing several key facets of modeling CICR, and have demonstrated the plausibility of a computationally inexpensive model for a cellular domain with many clusters, there is still much to be learned. Open questions include:

- Is the continuum approximation a reasonable assumption? How does a continuous diffusion model of CICR compare to a molecular dynamics model?
- Are there situations in which the assumptions of instantaneous equilibration and constant buffers break down? Are these situations biologically realistic?
- The curves in Figure 2.8 (point source vs. uniform flux) don't match as closely as might be desired, implying there may be significant error in the concentration at the channel opening. Why does this discrepancy arise? Can the implementation of the channel flux be improved further?
- Is cooperativity important for channel binding and dissociation reactions? What role does it play in the overall picture?
- Using clusters as the fundamental stochastic object instead of channels has so far resulted only in very rough approximations to results of other models. How can this approach be improved? Can it produce quantitatively useful results?

Appendix

A

The Gillespie-Rüdiger Algorithm

A.1 Motivation

Individual chemical reactions taking place on a relatively small scale can produce effects on a much larger scale. In calcium channel dynamics, a single molecule binding to or dissociating from a receptor can have a dramatic impact on the diffusion dynamics (by causing a channel to open or close). In order to adequately capture such a phenomenon, it is therefore desirable to model the individual reactions stochastically, and on a timescale where no more than one reaction occurs per stochastic timestep.

On the other hand, the individual reactions can take place on a much shorter timescale than the large-scale effects they produce. Diffusion of calcium ions away from an open channel can be much slower than the random binding and dissociation of ions from channel receptors. When modeling reactions numerically, in order to reduce computational cost, it is desirable to maximize the timestep used for modeling the stochastic process, especially when the stochastic process is coupled to a slower process in this way. A traditional Markov chain modeling a Poisson process does not achieve this since, by definition, most timesteps will not see anything happen.

Gillespie (1977) devised an algorithm to model stochastic processes whereby each stochastic timestep sees precisely one reaction take place, striking a balance between these two aims. The algorithm does this by, instead of fixing a stochastic timestep and computing what happens during this timestep, computing each timestep probabilistically. Specifically, each timestep is chosen to be the time between the most recent reaction and the next one. The nature of the next reaction is then also determined probabilistically.

Mathematically, this is done by indexing the possible reactions $i = 1, \cdots, n$ and drawing two random numbers $r_1, r_2 \in U(0, 1)$. We seek the stochastic timestep τ

and the index of the next reaction j, which are determined by

$$\tau = \frac{1}{\alpha} \ln\left(\frac{1}{r_1}\right)$$

and

$$\frac{1}{\alpha}\sum_{i=1}^{j-1} \alpha_i < r_2 \leq \frac{1}{\alpha}\sum_{i=1}^{j} \alpha_i$$

where α_i is the reaction rate for the i^{th} reaction and $\alpha = \sum_{i=1}^{n} \alpha_i$. The computed values of τ and j are then used to evolve the system from time t_0 to time $t_0 + \tau$: if the system is in state X at time t_0, and the reaction R_j takes the system from the state X to $R_j(X)$, then the numbers τ and j tell us that the system remains in state X for $t_0 \leq t < t_0 + \tau$ and is in state $R_j(X)$ at time $t = t_0 + \tau$.

The primary drawback to this algorithm is that it only considers reaction rates that are constant between reactions. In modeling calcium channel dynamics, diffusion dictates that the calcium concentration be a continuous function of time. Since molecular binding rates depend on the quantity of species present, this means that the rate of the binding of calcium to channel receptors must also depend continuously on time.

Alfonsi et al. (2005), therefore, extended Gillespie's algorithm to include reaction rates $\alpha_i = \alpha_i(t)$ that depend on time. Alfonsi's results for determining τ and j are as follows:

$$\int_{t_0}^{t_0+\tau} \alpha(t)dt = \ln\left(\frac{1}{r_1}\right)$$

and

$$\frac{1}{\alpha(t_0+\tau)}\sum_{i=1}^{j-1} \alpha_i(t_0+\tau) < r_2 \leq \frac{1}{\alpha(t_0+\tau)}\sum_{i=1}^{j} \alpha_i(t_0+\tau)$$

where t_0 is the time at which the most recent reaction occurred. Rüdiger et al. (2007)

provide a method for numerically computing τ from this equation and adapt this approach specifically for the framework of calcium ion channels. Rüdiger's algorithm for computing τ is examined at the end of this appendix.

In this appendix, we will start with a physical consideration of molecular reactions. We will then derive from first principles a probability distribution $P(\tau, j; t_0)$ for the occurrence of the first reaction after time t_0. From P, we will then derive the results given above, and demonstrate that they permit an algorithm for computing τ and j in a way that can be implemented in numerical models of chemical reactions.

We will first recreate the derivation of Gillespie (1977) and verify these results in the case that reaction rates are time-independent between reactions, and then show how to generalize to the time-dependent case, as is done by Alfonsi et al. (2005).

A.2 Setup

Suppose we have a chemical system with n species of reactants, $S_1, S_2, \cdots, S_n$, with respective numbers of molecules $N_1, N_2, \cdots, N_n$, and that there are m different possible reactions, $R_1, R_2, \cdots, R_m$, between these molecules, with the j^{th} reaction given by

$$R_j := \quad a_{j,1}S_1 + a_{j,2}S_2 + \cdots + a_{j,n}S_n \rightarrow \text{products}$$

We wish to determine the reaction rates α_j corresponding to each reaction.

The probability that a reaction of type R_j will take place in the time interval $(t, t + dt)$ is the probability that a particular set of R_j reactants react in that time interval times the number of possible different sets of R_j reactants. For example, suppose R_1 is characterized by

$$S_1 + S_2 \rightarrow S_3$$

The probability of one particular molecule of species S_1 and one particular molecule of species S_2 reacting in the time interval $(t, t + dt)$ is given by $c_1 dt$ where c_1 is a constant that depends only on the properties of the reactants and the temperature of the system. In a state of thermal equilibrium, c_1 is truly constant. Details about the constant c_1 may be found in (Gillespie, 1977).

Now, the probability of any reaction of this type occurring is the reaction probability of a single set of reactants multiplied by the number of possible reactant sets. The number of distinct reactant pairs in this case is simply $N_1 N_2$, and so the probability of an R_1 type reaction occurring in $(t, t + dt)$ is given by

$$N_1 N_2 c_1 dt$$

Note that the product S_3 has no bearing on the dynamics of the reaction.

Consider now the reaction R_2 characterized by

$$2S_1 \to S_4$$

with reaction probability constant c_2. (As before, the product S_4 is completely arbitrary.) The number of possible reactant pairs in this case is

$$\binom{N_1}{2} = \frac{N_1(N_1-1)}{2}$$

and so the probability of an R_2 type reaction occurring in the interval $(t, t+dt)$ is given by

$$\frac{1}{2}N_1(N_1-1)c_2dt$$

In general, if the reaction R_j is characterized by

$$a_{j,1}S_1 + a_{j,2}S_2 + \cdots + a_{j,n}S_n \to \text{products}$$

with reaction probability constant c_j, the probability of this kind of reaction occurring in $(t, t+dt)$ will be

$$\alpha_j dt \equiv \binom{N_1}{a_{j,1}}\binom{N_2}{a_{j,2}}\cdots\binom{N_n}{a_{j,n}}c_j dt$$

Note that because the c_j are constant and the N_j only change when there is a reaction (assuming a closed system), then the α_j are constant between reactions.

A.3 The probability distribution

We are interested in the probability distribution for the occurrence of the next reaction: the time at which it will take place, and the kind of reaction it will be. Hence we define[1] $P(\tau, j; t)$ such that $P(\tau, j; t)d\tau$ is the probability that the next reaction that occurs after time t will be in the interval $(t+\tau, t+\tau+d\tau)$ and will be of type R_j, given species quantities $N_1, N_2, \cdots, N_n$ at time t. Note that if we assume only one reaction can occur in an infinitesimal time interval $(t, t+dt)$, then $P(0, j; t) = \alpha_j$ by definition.

To compute $P(\tau, j; t)$, we first define $P_0(\tau; t)$ to be the probability that no reaction occurs in $(t, t+\tau)$. Then the probability that the next reaction after time t occurs in $(t+\tau, t+\tau+d\tau)$, and is of type R_j is equal to the probability that no reaction occurs in $(t, t+\tau)$ multiplied by the probability that an R_j reaction occurs in $(t+\tau, t+\tau+d\tau)$, i.e.,

$$P(\tau, j; t)d\tau = P_0(\tau; t)P(0, j; t+\tau)d\tau = P_0(\tau; t)\alpha_j d\tau$$

Computing $P_0(\tau; t)$ is straightforward. First we note that the probability of no reaction occurring in $(t, t+dt)$ is

$$P_0(t+dt; t) = 1 - \sum_{j=1}^{m} \alpha_j dt \equiv 1 - \alpha dt$$

So then

$$P_0(\tau + d\tau; t) = P_0(\tau; t)P_0(\tau + d\tau; \tau) = P_0(\tau; t) \cdot (1 - \alpha d\tau)$$

[1] The parameter t is unimportant for now, since the rates α_j are constant between reactions, but it will become useful later when we no longer take the α_j to be constant and so we include it here for consistency.

Thus

$$\frac{1}{P_0(\tau;t)}\frac{P_0(\tau+d\tau;t)-P_0(\tau;t)}{d\tau}=-\alpha$$

In the limit as $d\tau \to 0$, we therefore have

$$\frac{d}{d\tau}\ln(P_0(\tau;t))=-\alpha$$

Integrating from 0 to τ, we have:

$$P_0(\tau;t)=P_0(0;t)e^{-\alpha\tau}$$

But $P_0(0;t)=1$ trivially, so we have

$$P_0(\tau;t)=e^{-\alpha\tau}$$

And finally,

$$P(\tau,j;t)=\alpha_j e^{-\alpha\tau}$$

provided τ and j take on appropriate values. That is:

$$P(\tau,j;t)=\begin{cases}\alpha_j e^{-\alpha\tau} & \text{for } 0\le\tau<\infty,\ j=1,2,\cdots,n\\ 0 & \text{otherwise}\end{cases}$$

and we have the probability density function for τ and j.

A.4 Sampling the variables: Gillespie's algorithm

Now that we have the probability density for τ and j, we wish to find a method for sampling these quantities. Achieving this is straightforward in this situation, since τ and j are independent with this distribution: we have $P(\tau, j; t) = f(\tau)g(j)$ with

$$f(\tau) = \begin{cases} \alpha e^{-\alpha\tau} & \text{for } 0 \leq \tau < \infty \\ 0 & \text{otherwise} \end{cases}$$

$$g(j) = \begin{cases} \frac{\alpha_j}{\alpha} & \text{for } j = 1, 2, \cdots, n \\ 0 & \text{otherwise} \end{cases}$$

and so P is simply the joint distribution for independent exponential and discrete random variables. Sampling these kinds of distributions is an elementary result, but we reproduce the process here for the purpose of comparison with the later result involving time-dependence.

For a one-dimensional, continuous distribution, such as $f(\tau)$, we sample τ in the usual way: let F be the cumulative distribution function for τ: $F(\tau) = \int_{-\infty}^{\tau} f(s)ds$. Then F takes on values from 0 to 1. Set $r = F(\tau)$. Then $\tau = F^{-1}(r)$, with the existence of the inverse function ensured by the continuity and monotonicity of F. Now, simply sample r uniformly on $(0, 1)$ and use this relation to get a value for τ.

To verify that this gives the desired result, we compute the probability that a value of τ sampled in this manner lies in the interval $(s, s + ds)$. By definition of the density function, we expect this probability to be $f(s)ds$. Now, the probability of τ lying in $(s, s + ds)$ is, by construction, the same as the probability of r lying in $(F(s), F(s + ds))$. Since r is uniform on $(0, 1)$, this is simply

$$F(s + ds) - F(s) = F'(s)ds = f(s)ds$$

as desired.

For the function, $f(\tau) = \alpha e^{-\alpha\tau}$, we have

$$F(\tau) = 1 - e^{-\alpha\tau}$$

and

$$F^{-1}(r) = -\frac{1}{\alpha}\ln(1-r)$$

Since r is sampled uniformly on $(0,1)$, r is statistically equivalent to $1-r$, and so we can slightly simplify this result:

$$F^{-1}(r) = \frac{1}{\alpha}\ln\left(\frac{1}{r}\right)$$

We follow a similar procedure for the discrete distribution, $g(j)$. In the case of a discrete "density", with $g(j) = p_j$ for $j \in \mathbb{N}$ and $\sum_{i=0}^{\infty} p_i = 1$, the cumulative distribution function is given by

$$G(j) = \sum_{i=0}^{j} p_i$$

To sample this distribution, we take r uniformly on $(0,1)$ as before, and choose the value of j that satisfies

$$G(j-1) < r \leq G(j)$$

To verify that this gives the desired result, we compute the probability that a sampled value of j will equal i. We expect this probability to be p_i. By definition, the probability that $j = i$ is the same as the probability that $G(j) = G(i)$, which by construction is the same as the probability that $G(i-1) < r \leq G(i)$. Since r is

uniform on $(0,1)$, this is the same as

$$G(i) - G(i-1) = \sum_{i'=0}^{i} p_{i'} - \sum_{i'=0}^{i-1} p_{i'} = p_i$$

as desired.

Thus, for the function, $g(j) = \frac{\alpha_j}{\alpha}$, we sample r uniformly on $(0,1)$ and then pick j such that

$$\frac{1}{\alpha}\sum_{i=1}^{j-1} \alpha_i < r \leq \frac{1}{\alpha}\sum_{i=1}^{j} \alpha_i$$

To summarize thus far, we have computed the probability that the next reaction after time t will occur in the interval $(t+\tau, t+\tau+d\tau)$ and will be of type R_j. This probability is given by $P(\tau, j; t)d\tau$ where

$$P(\tau, j; t) = \begin{cases} \alpha_j e^{-\alpha\tau} & \text{for } 0 \leq \tau < \infty, j = 1, 2, \cdots, n \\ 0 & \text{otherwise} \end{cases}$$

We have shown that to sample τ and j from this distribution, we can sample r_1 and r_2 uniformly on $(0,1)$ and then compute τ by

$$\tau = \frac{1}{\alpha} \ln\left(\frac{1}{r_1}\right)$$

and pick j such that

$$\frac{1}{\alpha}\sum_{i=1}^{j-i} \alpha_i < r_2 \leq \frac{1}{\alpha}\sum_{i=1}^{j} \alpha_i$$

This method is Gillespie's algorithm.

A.5 Time dependence

Thus far, everything has assumed a closed, well-mixed system wherein the numbers $N_1, N_2, \cdots, N_n$ do not change between reactions and hence the α_j can be considered constant when computing details about the next reaction. Such a situation is not always possible, however. In particular, if there is a concentration gradient of any of the reactant species, an external source of reactant species, or any other method by which a species can enter or leave a volume of interest, the α_j, which depend on the quantities of the reactants, can change continuously in time, even between reactions. In this section, we will assume time-dependent reaction rates, attempt to follow the same procedure as in the proceeding sections, and highlight the differences that arise and how they may be treated. A thorough treatment of the time-dependent cast may also be found in (Alfonsi et al., 2005).

Consider the previous situation with the one alteration that the α_j now depend on time, i.e., $\alpha_j \equiv \alpha_j(t)$ and $\alpha \equiv \alpha(t)$. Computing $P(\tau, j; t)$ is identical in most regards. However, in computing $P_0(\tau; t)$, we have $P(0, j; t) = \alpha_j(t)$, and so we obtain the equation

$$\frac{d}{d\tau} \ln(P_0(\tau; t)) = -\alpha(t + \tau)$$

which has the solution

$$P_0(\tau; t) = e^{-\int_t^{t+\tau} \alpha(s) ds}$$

and so then the density function P becomes

$$P(\tau, j; t) = \begin{cases} \alpha_j(t + \tau) e^{-\int_t^{t+\tau} \alpha(s) ds} & \text{for } 0 \leq \tau < \infty,\ j = 1, 2, \cdots, n \\ 0 & \text{otherwise} \end{cases}$$

Obtaining this result required little deviation from the previous approach, but now we encounter a difficulty: τ and j are no longer independent random variables!

Before, we could just factor the exponential distribution for τ and the discrete distribution for j and treat them separately, but now the discrete factor α_j depends on τ as well. Physically, this is exactly what we expect; since the reaction rates are changing in time, so too should the relative probabilities of the different reaction types.

We may not be able to separate P, but we can still do something similar: Suppose we have a joint density $f(x, y)$ where the random variables X and Y are not independent. We use the marginal density for X, $f_X(x) \equiv \int_{-\infty}^{\infty} f(x, y)dy$, and use the same inversion algorithm as before. That is,

$$r_1 = F_X(x) = \int_{-\infty}^{x} f_X(x')dx'$$

and so, picking r_1 uniformly on $(0, 1)$, we set

$$x = F_X^{-1}(r_1)$$

Next, we use the conditional density for y given x,

$$f_{X=x}(y) \equiv \frac{f(x, y)}{f_X(x)}$$

and proceed similarly:

$$r_2 = F_{X=x}(y) = \int_{-\infty}^{y} f_{X=x}(y')dy'$$

and so, picking r_2 uniformly on $(0, 1)$, we set

$$y = F_{X=x}^{-1}(r_2)$$

To verify that this gives the desired result, we compute the probability

$$\text{Prob}(x' < x < x' + dx' \text{ and } y' < y < y' + dy')$$

with x and y sampled as described. We expect this probability to be equal to $f(x', y')dx'dy'$. The above probability is of course the same as

$$\text{Prob}(x' < x < x' + dx') \cdot \text{Prob}(y' < y < y' + dy' | x' < x < x' + dx')$$

which, by construction of r_1 and r_2, is equal to

$$\text{Prob}(F_X(x') < r_1 < F_X(x' + dx')) \cdot \text{Prob}(F_{X=x}(y') < r_2 < F_{X=x}(y' + dy'))$$

Since r_1 and r_2 are sampled uniformly, this is equal to

$$(F_X(x' + dx') - F_X(x')) \cdot (F_{X=x}(y' + dy') - F_{X=x}(y'))$$

$$\begin{aligned} &= f_X(x')dx' \cdot f_{X=x}(y')dy' \\ &= f_X(x')\frac{f(x', y')}{f_X(x')}dx'dy' \\ &= f(x', y')dx'dy' \end{aligned}$$

as desired.

If either or both of x and y take on discrete values, we can use the same approach, but with the discrete formulation as presented earlier. This will be illustrated in applying this technique to our particular distribution. Recall:

$$P(\tau, j; t) = \begin{cases} \alpha_j(t + \tau)e^{-\int_t^{t+\tau} \alpha(s)ds} & \text{for } 0 \leq \tau < \infty,\ j = 1, 2, \cdots, n \\ 0 & \text{otherwise} \end{cases}$$

We first sample τ and then, given the fixed value for τ, sample j. We have:

$$\begin{aligned} f_T(\tau) &= \sum_{j=1}^{m} P(\tau, j; t) \\ &= \sum_{j=1}^{m} \alpha_j(t+\tau) e^{-\int_t^{t+\tau} \alpha(s) ds} \\ &= e^{-\int_t^{t+\tau} \alpha(s) ds} \sum_{j=1}^{m} \alpha_j(t+\tau) \\ &= \alpha(t+\tau) e^{-\int_t^{t+\tau} \alpha(s) ds} \end{aligned}$$

so then

$$\begin{aligned} F_T(\tau) &= \int_{-\infty}^{\tau} f_T(s) ds \\ &= 1 - e^{-\int_t^{t+\tau} \alpha(s) ds} \end{aligned}$$

and so, setting $r_1 = F_T(\tau)$:

$$\begin{aligned} r_1 &= 1 - e^{-\int_t^{t+\tau} \alpha(s) ds} \\ \int_t^{t+\tau} \alpha(s) ds &= -\ln(1 - r_1) \end{aligned}$$

or equivalently,

$$\int_t^{t+\tau} \alpha(s) ds = \ln\left(\frac{1}{r_1}\right)$$

In the case that α does not depend on time, the integral evaluates to $\alpha\tau$, and so this result reduces exactly to the time-independent result.

We have derived the sampling equation for τ, but we have now encountered another difficulty: this equation is not easily solved for τ; the integral in general will not be able to be evaluated analytically, and so the left-hand side of this equation will not be invertible. We need another method to find τ.

A.6 Solving the integral: Rüdiger's algorithm

We have just shown that

$$\int_t^{t+\tau} \alpha(s)ds = \ln\left(\frac{1}{r_1}\right)$$

and wish to solve this equation for τ. If we define $g(\tau) = \int_t^{t+\tau} \alpha(s)ds$ and $\xi = \ln(\frac{1}{r_1})$, we want to solve $g(\tau) = \xi$ for τ, but g is in general not a function which is easily invertible. However, g is necessarily continuous and nondecreasing (since $\alpha \geq 0$), so there exists[2] a unique[3] value of τ that solves this equation, and we can find it simply by increasing τ until $g(\tau) = \xi$. This can be done easily by converting the integral equation for g into the initial value problem

$$\dot{g}(\tau) = \alpha(t+\tau); \quad g(0) = 0$$

and numerically integrating forward until the desired value for τ is found. This method for computing τ is the crux of Rüdiger's adaptation of the Gillespie algorithm.

Now that we have a method for computing τ, it remains to sample j conditionally

[2]It is conceivable that g asymptotically approaches some value less than ξ, but such situations would require the reaction rates to decay to zero, and would therefore require at least one species of reactant to evacuate the domain of interest entirely. Such a situation would require a different modeling approach.

[3]It is also conceivable that there may be be intervals on which g is constant, but on these intervals, the reaction rates again would necessarily all be zero. Even so, the number of such plateaus is necessarily countable, and so the set of them has measure zero.

given this value of τ. We have:

$$\begin{aligned} f_{T=\tau}(j) &= \frac{P(\tau, j; t)}{f_T(\tau)} \\ &= \frac{\alpha_j(t+\tau)e^{-\int_t^{t+\tau}\alpha(s)ds}}{\alpha(t+\tau)e^{-\int_t^{t+\tau}\alpha(s)ds}} \\ &= \frac{\alpha_j(t+\tau)}{\alpha(t+\tau)} \end{aligned}$$

So, given a value for τ, sampling j is exactly the same as before: given r_2 sampled uniformly from $(0, 1)$, pick j such that

$$\frac{1}{\alpha(t+\tau)}\sum_{i=1}^{j-1}\alpha_i(t+\tau) < r_2 \leq \frac{1}{\alpha(t+\tau)}\sum_{i=1}^{j}\alpha_i(t+\tau)$$

We have therefore demonstrated the Gillespie-Rüdiger algorithm in both the time-independent case and the time-dependent case.

Appendix

B

Analytic Steady-State Solution due to a Single Open Channel

B.1 Overview

It is desirable to have an analytic solution for the steady-state profile of a single open channel as it offers both a method of computation that can be incorporated into different models, as well as a benchmark for comparison. In this appendix, we will offer a brief derivation for the steady-state profile due to a localized source, originally printed in (Neher, 1986).

Assume the flux source has zero physical extent and is embedded in an infinite flat membrane. We define the channel's location to be the origin, and allow calcium to diffuse through the entire half-space exterior to the membrane. Then the calcium concentration, as a function of distance from the channel, r, is given by

$$c(r) = c_0 + \frac{I}{4\pi DF}\frac{e^{-\sqrt{\frac{k^+ b}{D}}r}}{r}$$

in this half-space, where c_0 is the base concentration of calcium when the channel is closed (and so the limiting concentration as $r \to \infty$), I is the open channel current, F is the Faraday constant, and the remaining quantities are as previously defined.

B.2 Setup and reduction

Recall the reaction-diffusion equation for c:

$$\frac{\partial c}{\partial t} = D\nabla^2 c + \sum_{i=s,m,e} \left(k_i^-(B_i - b_i(\mathbf{r})) - k_i^+ b_i(\mathbf{r})c(\mathbf{r})\right) + \sum_j \phi_j(t)\delta(\mathbf{r} - \mathbf{r}_j)$$

For simplicity, for the rest of this appendix, we will assume only one species of buffer. Then:

$$\frac{\partial c}{\partial t} = D\nabla^2 c - k^+ b(\mathbf{r})c(\mathbf{r}) + k^-(B - b(\mathbf{r})) + \sum_j \phi_j(t)\delta(\mathbf{r} - \mathbf{r}_j)$$

When all channels are closed, there exists an equilibrium concentration c_0 given by

$$k^+ b_0 c_0 = k^-(B - b_0)$$

or

$$c_0 = K\frac{B - b_0}{b_0}$$

where b_0 is the buffer concentration at equilibrium and $K \equiv \frac{k^-}{k^+}$ is the dissociation constant for the calcium-buffer reaction. (In actuality, models often specify B and c_0 first, since those are the variables specified in experiments, and then let b_0 be a derived quantity, but this is unimportant here.)

Since we desire a steady-state profile for a single channel, we naturally seek a full solution of the form $c(\mathbf{r}, t) = c(r) = c_0 + f(r)$. The angular independence arises from a simple consideration of geometry: the two simplest models involve either a channel far from any boundaries (in which case full radial symmetry is immediately apparent) or a channel embedded in a membrane. The membrane can be locally approximated as flat, in which case symmetry dictates that locally, the solution will be everywhere twice the "free channel" solution, and thus still radially symmetric in the half-space on the outside of the membrane. Substituting this ansatz into the full

equation yields a reduced equation for f:

$$D\left(\frac{d^2f}{dr^2}+\frac{2}{r}\frac{df}{dr}\right)=k^+b_0f$$

$$\frac{d^2f}{dr^2}+\frac{2}{r}\frac{df}{dr}=\frac{k^+b_0}{D}f\equiv\mu^2f$$

This equation has the two solutions $\frac{1}{r}e^{-\mu r}$ and $\frac{1}{r}e^{\mu r}$. Since $\mu=\sqrt{\frac{k^+b_0}{D}}>0$, the latter is unphysical for large r and so we discard it. This leaves us with the full solution

$$c(r)=c_0+\frac{A}{r}e^{-\mu r}$$

where it remains to determine the value of A.

B.3 Flux condition

We have determined that the steady-state solution has the form

$$c(r) = c_0 + \frac{A}{r}e^{-\mu r}$$

where $\mu = \sqrt{\frac{k^+ b_0}{D}}$, and we seek to determine A.

To do so, we consider a flux condition at $r = 0$. Suppose the open channel exhibits a steady current I. Then the molar flux per unit time out of the channel is given by $\phi = \frac{I}{2F}$ where $F = 96485\ \mathrm{C \cdot mol^{-1}}$ is the Faraday constant and the factor of 2 is due to the fact that a calcium ion has a charge of +2. Assume the geometry in which the channel is embedded in an infinite planar membrane, and consider a hemisphere of radius R centered on the channel. We integrate the steady-state equation over this space:

$$0 = \iiint_V D\nabla^2 c\, dV + \iiint_V \phi\delta^3(\mathbf{r})\, dV + \iiint_V (\text{other terms})\, dV$$

$$0 = D \oiint_{\partial V} \nabla c \cdot d\mathbf{S} + \phi + \iiint_V (\text{other terms})\, dV$$

$$0 = D \cdot 2\pi r^2 \frac{dc}{dr}\bigg|_{r=R} + \phi + \iiint_V (\text{other terms})\, dV$$

noting that there is no flux through the membrane.

If we let $R \to 0$, the "other terms" vanish, and we have

$$D \cdot 2\pi r^2 \frac{dc}{dr}\bigg|_{r=0} = -\phi = -\frac{I}{2F}$$

or

$$r^2 \frac{dc}{dr}\bigg|_{r=0} = -\frac{I}{4\pi DF}$$

Applying this to our solution:

$$\begin{aligned} r^2 \frac{dc}{dr}\bigg|_{r=0} &= r^2 \left(c_0 + \frac{A}{r} e^{-\mu r} \right)' \bigg|_{r=0} \\ &= r^2 (-e^{-\mu r}) \left(\frac{A}{r^2} + \mu \frac{A}{r} \right) \bigg|_{r=0} \\ &= -A e^{-\mu r} (1 + \mu r) \big|_{r=0} \\ &= -A \end{aligned}$$

Therefore $A = \frac{I}{4\pi DF}$ and we have

$$c(r) = c_0 + \frac{I}{4\pi DF} \frac{e^{-\sqrt{\frac{k+b}{D}} r}}{r}$$

and so we have successfully computed the steady-state solution.

Bibliography

A. Alfonsi, E. Cances, G. Turinici, B. D. Ventura, and W. Huisinga. Exact simulation of hybrid stochastic and deterministic models for biochemical systems. *ESAIM Proc.*, 14:1–13, 2005.

F. J. Amador, L. Kimlicka, P. B. Stathopulos, G. M. C. Gasmi-Seabrook, D. H. Maclennan, F. Van Petegem, and M. Ikura. Type 2 ryanodine receptor domain A contains a unique and dynamic -helix that transitions to a -strand in a mutant linked with a heritable cardiomyopathy. *J Mol Biol*, 425(21):4034–46, Nov 2013. doi: 10.1016/j.jmb.2013.08.015.

I. Bezprozvanny and B. E. Ehrlich. Inositol (1,4,5)-trisphosphate (InsP3)-gated Ca channels from cerebellum: conduction properties for divalent cations and regulation by intraluminal calcium. *J Gen Physiol*, 104(5):821–56, Nov 1994.

M. Bootman, E. Niggli, M. Berridge, and P. Lipp. Imaging the hierarchical Ca2+ signalling system in HeLa cells. *J Physiol*, 499 (Pt 2):307–14, Mar 1997.

N. Callamaras and I. Parker. Radial localization of inositol 1,4,5-trisphosphate-sensitive Ca2+ release sites in Xenopus oocytes resolved by axial confocal linescan imaging. *J Gen Physiol*, 113(2):199–213, Feb 1999.

N. Callamaras, J. S. Marchant, X. P. Sun, and I. Parker. Activation and co-ordination of InsP3-mediated elementary Ca2+ events during global Ca2+ signals in Xenopus oocytes. *J Physiol*, 509 (Pt 1):81–91, May 1998.

Q. A. Dang and M. Ehrhardt. On Dirac delta sequences and their generating functions. *Applied Mathematics Letters*, 25(12):2385–2390, July 2012.

G. W. De Young and J. Keizer. A single-pool inositol 1,4,5-trisphosphate-receptor-based model for agonist-stimulated oscillations in Ca2+ concentration. *Proc Natl Acad Sci U S A*, 89(20):9895–9, Oct 1992.

G. Dupont, L. Combettes, G. S. Bird, and J. W. Putney. Calcium oscillations. *Cold Spring Harb Perspect Biol*, 3(3), Mar 2011. doi: 10.1101/cshperspect.a004226.

D. T. Gillespie. Exact stochastic simulation of coupled chemical reactions. *J Phys Chem*, 8:2340, 1977.

Z. Hannaert-Merah, L. Combettes, J. F. Coquil, S. Swillens, J. P. Mauger, M. Claret, and P. Champeil. Characterization of the co-agonist effects of strontium and calcium on myo-inositol trisphosphate-dependent ion fluxes in cerebellar microsomes. *Cell Calcium*, 18(5):390–9, Nov 1995.

Y. Jiang, A. Lee, J. Chen, V. Ruta, M. Cadene, B. T. Chait, and R. MacKinnon. X-ray structure of a voltage-dependent K+ channel. *Nature*, 423(6935):33–41, May 2003. doi: 10.1038/nature01580.

D. O. Mak, S. McBride, and J. K. Foskett. Inositol 1,4,5-tris-phosphate activation of inositol tris-phosphate receptor Ca2+ channel by ligand tuning of Ca2+ inhibition. *Proc Natl Acad Sci U S A*, 95(26):15821–5, Dec 1998.

E. Neher. Concentration profiles of intracellular calcium in the presence of a diffusible chelator. In U. Heinemann, M. Klee, E. Neher, and W. Singer, editors, *Calcium Electrogenesis and Neuronal Functioning*, pages 80–96. Berlin: Springer, 1986.

I. Parker and Y. Yao. Ca2+ transients associated with openings of inositol trisphosphate-gated channels in Xenopus oocytes. *J Physiol*, 491 (Pt 3):663–8, Mar 1996.

S. Rüdiger, J. W. Shuai, W. Huisinga, C. Nagaiah, G. Warnecke, I. Parker, and M. Falcke. Hybrid stochastic and deterministic simulations of calcium blips. *Biophys J*, 93(6):1847–57, Sep 2007. doi: 10.1529/biophysj.106.099879.

M. Sanson, C. Ingueneau, C. Vindis, J.-C. Thiers, Y. Glock, H. Rousseau, Y. Sawa, Y. Bando, Z. Mallat, R. Salvayre, and A. Nègre-Salvayre. Oxygen-regulated protein-150 prevents calcium homeostasis deregulation and apoptosis induced by oxidized LDL in vascular cells. *Cell Death Differ*, 15(8):1255–65, Aug 2008. doi: 10.1038/cdd.2008.36.

A. Skupin, H. Kettenmann, and M. Falcke. Calcium signals driven by single channel noise. *PLoS Comput Biol*, 6(8), 2010. doi: 10.1371/journal.pcbi.1000870.

G. D. Smith, J. Wagner, and J. Keizer. Validity of the rapid buffering approximation near a point source of calcium ions. *Biophys J*, 70(6):2527–39, Jun 1996. doi: 10.1016/S0006-3495(96)79824-7.

X. P. Sun, N. Callamaras, J. S. Marchant, and I. Parker. A continuum of InsP3-mediated elementary Ca2+ signalling events in Xenopus oocytes. *J Physiol*, 509 (Pt 1):67–80, May 1998.

S. Swillens, P. Champeil, L. Combettes, and G. Dupont. Stochastic simulation of a single inositol 1,4,5-trisphosphate-sensitive Ca2+ channel reveals repetitive openings during 'blip-like' Ca2+ transients. *Cell Calcium*, 23(5):291–302, May 1998.

S. Swillens, G. Dupont, L. Combettes, and P. Champeil. From calcium blips to calcium puffs: theoretical analysis of the requirements for interchannel communication. *Proc Natl Acad Sci U S A*, 96(24):13750–5, Nov 1999.

D. Thomas, P. Lipp, M. J. Berridge, and M. D. Bootman. Hormone-evoked elementary Ca2+ signals are not stereotypic, but reflect activation of different size channel clusters and variable recruitment of channels within a cluster. *J Biol Chem*, 273(42):27130–6, Oct 1998.

K. Thurley and M. Falcke. Derivation of Ca2+ signals from puff properties reveals that pathway function is robust against cell variability but sensitive for control. *Proc Natl Acad Sci U S A*, 108(1):427–32, Jan 2011. doi: 10.1073/pnas.1008435108.

H. M. Viola and L. C. Hool. Cross-talk between L-type Ca2+ channels and mitochondria. *Clin Exp Pharmacol Physiol*, 37(2):229–35, Feb 2010. doi: 10.1111/j.1440-1681.2009.05277.x.

J. Watras, I. Bezprozvanny, and B. E. Ehrlich. Inositol 1,4,5-trisphosphate-gated channels in cerebellum: presence of multiple conductance states. *J Neurosci*, 11 (10):3239–45, Oct 1991.